Drug Delivery and Translational Research
https://doi.org/10.1007/s13346-025-01916-7

ORIGINAL ARTICLE

Nasal inhalation of antiviral microparticulate powders to target early infection of upper airways

Sabrina Banella[1,2] · Eride Quarta[3] · Martina Brandolini[4,5] · Laura Grumiro[4,5] · Vittorio Sambri[4,5] · Giovanna Trevisi[6] · Ruggero Bettini[3] · Paolo Colombo[3,7] · Francesca Buttini[3] · Fabio Sonvico[3] · Georgeta Caraua[3] · Alessandra Rossi[3] · Gaia Colombo[1]

Accepted: 28 June 2025

Abstract

During the COVID-19 pandemic, several compounds among which chloroquine diphosphate (CqP), have been repurposed as anti-SARS-CoV-2 drugs. Critically, studies were most often performed by systemic drug administration, whereas the early viral infection of human body appeared in the upper respiratory tract. This research addressed the delivery strategy for depositing a powder aerosol of CqP onto the upper airways by a nasal inhalation act. By formulating the drug as nasal microparticulate aerodynamic powder, the loco-regional application of particle aerosol concentrates the drug primarily on the upper airway epithelia where the virus replicates. Nasal microparticulate powders of CqP, with and without excipients, were engineered by spray drying, obtaining particle size, density and morphology suitable for aerosolization and deposition onto the upper respiratory tract. The powders were loaded into a pre-metered device for oral inhalation of dry powders that was innovatively actuated by a nasal sharp sniff. The generated nasal airflow, measured in healthy volunteers, enabled powder dose emission from the inhaler. Chloroquine diphosphate microparticles, deposited on rabbit nasal mucosa ex vivo, led in less than 45 min to CqP concentrations within the epithelial cells between 30–70 mM. The in vitro CqP concentrations inhibiting SARS-CoV-2 replication, were in the μM range. The virus inhibition studied in Vero E6 cells was further enhanced when the cells were pre-treated with the drug powder before infection. In conclusion, the simple nasal sniff of an antiviral aerodynamic powder could be active against airborne viral early infection, limiting the exposition of the whole body to undesired drug effects.

Sabrina Banella and Eride Quarta contributed equally to this work.

✉ Gaia Colombo
clmgai@unife.it

1 Department of Life Sciences and Biotechnology, University of Ferrara, Via Fossato di Mortara 19, 44121 Ferrara, Italy

2 Department of Diagnostics and Public Health, University of Verona, Piazzale L. Scuro 10, 37134 Verona, Italy

3 Food and Drug Department, University of Parma, Parco Area delle Scienze 27/A, 43124 Parma, Italy

4 Unit of Microbiology, The Greater Romagna Area Hub Laboratory, Piazza della Liberazione 60, 47522 Cesena, Italy

5 Department of Medical and Surgical Sciences (DIMEC), University of Bologna, Via G. Massarenti 9, 40138 Bologna, Italy

6 Institute of Materials for Electronics and Magnetism, IMEM-CNR, Parco Area delle Scienze 37/A, 43124 Parma, Italy

7 PlumeStars Srl, C/O Food and Drug Department, University of Parma, Parco Area delle Scienze 27/A, 43124 Parma, Italy

Published online: 15 July 2025

Keywords Respiratory virus · Antiviral · Chloroquine diphosphate · Nasal microparticulate powder · Nasal sniff.

Introduction

In spring 2020, the first months of COVID-19 pandemic, it was published that the infection by SARS-CoV-2 evolved in three stages, the most critical one being the life-threatening hyperinflammatory Stage III (Fig. 1) [1].

During the pandemic, patients admitted into hospitals with a severe pulmonary disease, essentially received medical treatments to counteract the inflammation and control the hyperreactive immune system. Similarly to the most common airborne diseases by respiratory viruses, the early infection at Stage I is the most obvious phase for an antiviral treatment. However, for almost two years, it was the least considered therapeutical target. Indeed, an individual with malaise and flu-like symptoms, consulting the general practitioner, did not receive prescriptions according to an early time antiviral protocol, but only symptomatic remedies. In 2021 in Italy the common prescription for the early mild disease in home setting were paracetamol or NSAIDs and to adopt a "vigilant waiting". Three years later, the last update of the NIH COVID-19 Treatment Guidelines (dated February 29, 2024) still recommended only symptom management in adult patients at low risk of progressing to severe COVID-19 (the guidance is no more available as the webpage was shut down on August 16th, 2024).

Researchers have repurposed several drugs for the management of SARS-CoV-2 to counteract the disease progression [2, 3]. A number of these substances with antiviral activity entered in clinical trials against SARS-CoV-2 infection, essentially by systemic administration on hospitalized patients experiencing the pulmonary phase of disease. Chloroquine, hydroxychloroquine, lopinavir, ritonavir, amantadine [4], and colchicine [5] have been administered orally or by injection with contradictory results [6, 7]. Remdesivir received emergency authorization as intravenous antiviral treatment for COVID-19 patients at the end of 2020 [8].

Notably, systemic administration yields to low concentrations of antiviral drug in the upper airway epithelia, which are the site of early infection, neglecting that a timely given antiviral agent could impactfully prevent disease worsening and pneumonia. Noteworthily, in the ECDC recommendations for antiviral treatment of a seasonal airborne viral infection like influenza, antiviral medicines should be prescribed for use within 48 h from symptom onset to maximize therapeutic benefits [9]. As a matter of fact, respiratory viruses infect the body primarily in the upper respiratory tract. Shooting them on site to prevent their progression to the lower airways, emerges as strategic [10, 11].

An antiviral nasal aerosol of drug microparticles, deposited onto the upper airway epithelia, could loco-regionally boost the active concentration where needed. The aerosol particles intimately coat the infected epithelium and dissolve for local fast drug absorption by cells. Thus, such a product would decrease the viral load in the early phase of disease, when virus replication is dominant. In fact, it is very instructive to know that saliva swab samples from patients showed a striking correlation between high virus levels and later hospitalization or death [12].

Hence, the hypothesis driving this research was that the virus must be tackled in the infected upper airways by providing a loco-regional delivery of powder aerosol to impede the lung invasion by replicated virions. As the early infection by SARS-CoV-2 embraces the upper airways, *i.e.*, nasal cavities, throat, pharynx, and larynx [13], the aim of this research was to study antiviral microparticulate powders that can be aerosolized to deposit onto the upper airway epithelia

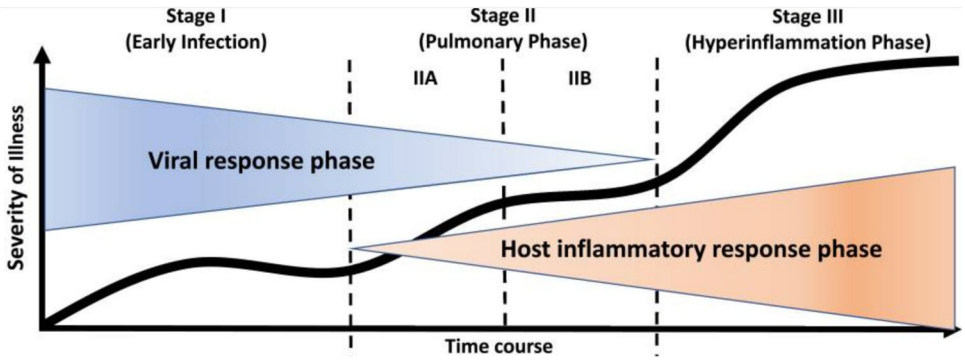

Fig. 1 Progression of COVID-19 severity *vs.* time course (reproduced with permission from [1])

by a nasal inspiration act. The objective was to provide high intracellular drug concentrations at the local level. In detail, microparticulate powders of the antimalarial chloroquine diphosphate (CqP) were formulated and combined with a commercial dry powder inhaler (DPI) for oral inhalation, never employed before for nasal use. Usually, nasal powders are insufflated or sprayed into the nostrils with nasal devices refraining from breathing, for localized deposition only within the nasal cavities. Here, aiming to a broader upper airway coverage, a short and sharp sniff [14] is the maneuver performed with a DPI appropriate for insertion into the nostril to deposit particles beyond the nasal cavity. By such nasal sniff of fine particles, we intend to create an aerosol enabling drug deposition over the whole upper airway epithelia. Chloroquine diphosphate is reported to have anti-SARS-CoV-2 activity [15–17]. For powder formulation, CqP was combined with zinc gluconate and lactoferrin aiming to enhance the effectiveness of upper airway deposition and antiviral action.

The engineered microparticulate powders constructed by spray drying, were combined with the pre-metered device Turbospin® [18]. This inhaler is designed for oral inhalation of pulmonary dry powders. It has a cylindrical mouthpiece adapter whose diameter can fit the nostril for sniffing (Fig. 2). The novelty is that the drug particle aerosol is produced by the airflow generated by a nasal inspiration act through the device. Despite the generated airflow is slower than the airflow rate of an oral inhalation, the nasal inhalation is expected capable to broaden the deposition of the micronized particles all over the upper respiratory tract and beyond, down to trachea. The nasal dose of antiviral chloroquine diphosphate will be at least one order of magnitude lower than the oral dose [19].

The pharmaceutical characteristics of the nasal powders were assessed in terms of geometric and aerodynamic particle size distributions at different airflow rates, in vitro drug release, ex vivo CqP permeation and accumulation within rabbit nasal mucosa. The antiviral activity of nasal CqP powders was tested on Vero E6 cells infected with SARS-CoV-2. In order to determine the airflow rate generated and the amount of powder emitted upon a nasal sharp sniff, a placebo microparticulate powder was administered to human volunteers.

Material and methods

Material

Chloroquine diphosphate (CqP; batch # 50–63-5, 3050) was purchased by Sigma Aldrich (Saint Louis, MO, USA). Zinc gluconate was purchased from A.C.E.F (Fiorenzuola d'Arda, Italy) and lactoferrin (80 kDa) was supplied by Sigma-Aldrich (Saint Louis, MO, USA). All solvents (water, acetonitrile, methanol) were HPLC-grade (Scharlab, Barcelona, Spain). Cell culture medium (EMEM) and supplements were purchased from EuroClone (Milan, Italy). HPMC extra-dry capsules for use in dry powder inhalers (Quali-V®-I, size #3), were provided by Qualicaps (Madrid, Spain), while the Turbospin® inhaler was a kind gift of PH&T (now NTC srl, Milan, Italy).

Methods

Nasal powder manufacturing by spray drying

Micronized nasal powders of chloroquine diphosphate, alone or combined with lactoferrin and/or zinc gluconate (Table 1), were manufactured on a Büchi B-290 spray dryer (BÜCHI Labortechnik AG, Flawil, Switzerland). The spray drying operating conditions were the same for all powders, namely: 600 l/h airflow rate, 35 m^3/h aspiration, 3 mL/min liquid feed rate and 0.7 mm nozzle. Inlet and outlet temperatures were 125 °C and 75 °C, respectively. The liquid feed was prepared by dissolving the drug and the other components in purified water to a final volume to keep the total solid concentration in the feed around 1% (w/v) for all formulations. The pH of the feed solutions was always between 4.5 and 5.5.

Analytical method for chloroquine diphosphate assay

A reverse-phase HPLC–UV method was developed in-house for determining chloroquine diphosphate content in the spray-dried powders as well as in samples from in vitro and ex vivo experiments. The apparatus was an Agilent 1200 series (Agilent, Santa Clara, CA, USA), equipped with an UV–Vis detector. The stationary phase was a Luna C18

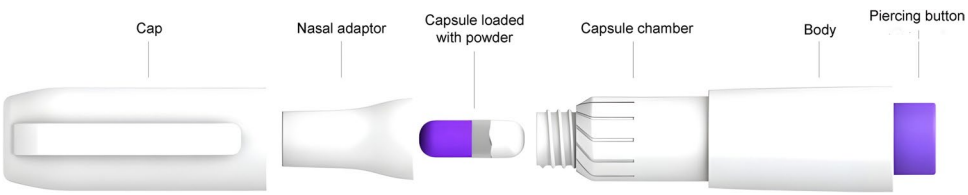

Fig. 2 Drawing of the oral/nasal dry powder inhaler Turbospin® (PH&T, now NTC Srl, Milan, Italy). The composing parts are depicted with the device in open setting for capsule loading

Table 1 Composition by weight of the three spray-dried powders: CqP monocomponent, CqP binary composite and ternary composite

Formulation	Chloroquine diphosphate (% w/w)	Zinc gluconate	Lactoferrin
CqP monocomponent	100	-	-
CqP binary composite	80	20	-
CqP ternary composite	70	18	12

column (3 µm, 4.6 × 300 mm; Phenomenex, Torrance, CA, USA). The mobile phase was a mixture of 25 mM potassium dihydrogen phosphate and acetonitrile (85:15), whose pH was adjusted to 2.5 ± 0.1 with orthophosphoric acid. The detection wavelength was set at 224 nm. Isocratic elution was carried out at 0.8 mL/min flow rate at room temperature; the injection volume was 10 µl. In these conditions, the retention time of CqP was 5.9 min. The method was validated according to the EMA Note for Guidance on Validation of Analytical Procedures: Text and Methodology (CPMP/ICH/381/95). The linearity was confirmed in the 7.5–250.0 µg/ml CqP concentration range. Method accuracy and precision were proven respectively by CqP recoveries > 98.5% and an RSD% of 0.68%.

The CqP standard solution was prepared in HPLC-grade water at about 1 mg/ml concentration. This solution was diluted with the mobile phase to CqP final concentrations between 40–50 µg/ml. Chloroquine diphosphate content of the powders was determined after dissolving an accurately weighed amount of spray-dried powder in 10 ml of HPLC-grade water. These sample solutions were diluted with mobile phase before analysis. Measurements were performed in triplicate for each powder.

Characterization of the solid state of the spray-dried nasal powders

Differential scanning calorimetry (DSC) analysis of the spray-dried powders was performed on a Mettler DSC821e instrument equipped with STARe software (Mettler Toledo, Columbus, OH, USA). Accurately weighed amounts (4–6 mg) of each powder were loaded into a 40 µl aluminum pan, which was then sealed and double pierced. Scans were performed between 25 and 200 °C at a heating rate of 10 °C/min under purging nitrogen atmosphere at 100 mL/min flow rate.

A TGA/DSC 1 STARe System (Mettler Toledo, Columbus, OH, USA) was used to quantify the percentage of residual humidity. The analysis was carried out on accurately weighed 4 mg samples of powder placed in an aluminum pan under nitrogen flow at 80 mL/min. The temperature was increased from 25 °C to 150 °C at a rate of 10 °C/min.

Powder X-ray diffraction (PXRD) was applied to determine the crystallinity degree of the spray-dried nasal powders compared to CqP raw material. The diffractograms were recorded on a D8 Advance diffractometer (Bruker, Karlsruhe, Germany) equipped with a Lynx-eye position sensitive detector using Cu Kα radiation (λ = 1.54178 Å) generated at 40 kV and 40 mA as X-ray source. Spectra were recorded in the 2θ range from 10° to 60° with a step size (2θ) of 0.02° and a counting time of 0.5 s.

Micromeritics of the spray-dried nasal powders

The spray-dried powders were characterized with respect to particle size distribution, morphology, bulk density, flowability. Particle geometric size was determined by the laser diffraction (LD) technique (Spraytec, Malvern Panalytical, Malvern, UK). About 10 mg of microparticulate powder sample were dispersed in 10 ml of 0.1% (w/v) Span 85 in cyclohexane. The analysis was carried out at 5% threshold obscuration.

Particle morphology was analyzed by Field Emission Scanning Electron Microscopy (FESEM) equipped with a Ga Focused Ion Beam (FIB) Auriga Compact (Zeiss, Oberkochen, Germany). The analyses were performed on the powders directly dispersed on the Carbon-tape, without metallization. SEM imaging was conducted with 1 kV acceleration voltage of the electron beam and FIB processing was carried out using ion beams with 20 pA and 30 kV current and acceleration voltage, respectively.

Untapped and tapped bulk densities (ρ) were determined according to the "Bulk density of powders" chapter (2.9.34) in the Ph. Eur. 11th. The measured bulk density values were then used to calculate the Carr index according to the following equation (Eq. 1):

$$Carr\ index(\%) = \frac{\rho_{tapped} - \rho_{untapped}}{\rho_{tapped}} \times 100 \quad (1)$$

A direct determination of the powder flow was also carried out by measuring the dynamic angle of repose of powders according to Buttini et al. [20]. Briefly, the powder was half-filled in a transparent 10 ml glass vial. Then, the vial was rotated in horizontal orientation around the main axis at 40 rpm to observe the powder avalanching from the bottom

of the vial. The arising angle between the sliding powder plane and the horizontal plane was measured as dynamic angle of repose (Φ) [21].

Measurements of the nasal airflow rate generated by powder inspiration in healthy volunteers

The nasal airflow rate generated by two male and two female volunteers (age range: 31-75y) was assessed by performing a nasal inspiration act (sharp sniff) through the Turbospin® dry powder inhaler (Fig. 2). The study was carried out upon approval by the Research Ethics Board of the University of Parma (prot. number 0145714, June 11th, 2024). Informed consent was obtained from all individual volunteers included in the study.

For safety and ethical reasons, a spray-dried mannitol respirable powder was used for this study, manufactured according to Quarta et al. [22] and characterized for $d_{v,50}$ (2.5 µm) and respirability (Fine Particle Fraction > 50%). 35.7 mg of such powder were loaded into a size #3 HPMC hard capsule. The capsule was manually inserted into the device chamber, located under the screwable mouthpiece elected as nasal adaptor to aerosolize the powder by a nasal sharp sniff. The airflow rate produced for dose extraction was recorded using a flow meter (Copley Scientific, Nottingham, UK) [23]. The amount of powder emitted was quantified gravimetrically as described below.

The volunteers were instructed on how to perform a nasal sharp sniff through the device, one per nostril. In detail, the device was weighed and the loaded capsule was pierced by pressing the dedicated button. Then, the device was inserted into a volumetric chamber connected to the flow meter, keeping the "nosepiece" emerging from the chamber [23]. The volunteers were asked to blow their nose prior to inhale. Next, they exhaled through the nose before inserting the "nosepiece" into the nostril. Keeping the other nostril closed by finger pressure, the nasal sharp sniff was executed. The resulting airflow made the pierced capsule rattle inside the chamber, enabling powder extraction as aerosol. Capsule rattling during inhalation assures the emission of the powder from the inhaler. After the first sniff, the amount of powder emitted was measured by weighing the device. Then, the set-up was re-assembled and the procedure repeated with the other nostril. The waiting time between the two sniffs by the volunteer was around 3 min. Any perception experienced by the subjects was recorded.

Aerodynamic assessment of the spray-dried nasal powders

The aerodynamic measurements were performed by using a Next Generation Impactor (NGI; Copley Scientific, Nottingham, UK). The cups of the impactor were coated by spraying and drying a solution of 2% (w/v) Tween 20 in ethanol to prevent particle bouncing. The NGI was connected to a vacuum pump (SCP5; Copley Scientific, Nottingham, UK) through a critical flow controller (TPK; Copley Scientific, Nottingham, UK). Airflow rates of 34 L/min and 65 L/min, measured with a DFM 2000 Flow Meter (Copley Scientific, Nottingham, UK), were applied to activate the Turbospin® device at 1 and 4 kPa pressure drop, respectively. The TPK actuation time was adjusted so that a 4-L air volume was drawn through the inhaler. Each capsule contained a mass of spray-dried nasal powder corresponding to 25 mg of CqP. Thus, powder loadings in the capsule were 25.5, 31.3 or 35.7 mg, depending on the drug content of the formulation. The powder deposited on the NGI stages was quantified by HPLC for CqP content. The emitted dose (ED) was calculated as the amount of drug leaving the device and entering the impactor. The mass median aerodynamic diameter (MMAD) was determined by plotting on a probability scale the cumulative undersize percent mass fraction collected from each stage, *vs.* the logarithm of the aerodynamic cut-off diameter of the stage. The fine particle dose (FPD) is the mass of drug particles with an aerodynamic diameter lower than 5 µm, as calculated from the log-probability plot equation. The fine particle fraction (FPF) was calculated as the percent ratio of the FPD to the ED.

In vitro dissolution rate of the spray-dried nasal powders

Powder dissolution rate was estimated by performing a diffusional transport experiment of CqP across a non-partitioning permeable membrane on which a weighed powder sample was deposited. Franz-type vertical diffusion cells were used (Vetrotecnica, Padova, Italy), comprising a top donor compartment separated from a bottom receptor compartment by a regenerated cellulose membrane (MW cut-off 12,000–14,000 Da, Dexstar Visking, Medicell International Ltd, London, UK). The receptor was filled with 4.7 ml of PBS pH 7.4 at 37 °C. The powder, evenly spread on the membrane surface, was wetted with 0.1 ml of the same buffer to reproduce the nasal mucosa wet environment. The CqP dose of 10 mg in the donor was constant among the different formulations.

Ex vivo permeation of chloroquine diphosphate across nasal rabbit mucosa

Vertical Franz-type cells were employed. The biological membrane was a specimen of nasal mucosa extracted from the nose septum of rabbit heads obtained from slaughterhouse waste (Pola srl, Finale Emilia, Italy). Mucosa extraction and cell assembly ended within 2 h from the animal's death [24, 25].

An accurately weighed amount of nasal powder containing 7.5 mg of CqP, was introduced in the donor. The powder was distributed on the mucosa as evenly as possible to cover all the available surface (0.58 cm^2) and wet with 0.1 ml of PBS pH 7.4. During the experiment, the assembled cell was kept at 37 °C in a thermostatic water bath with the receptor constantly stirred. A sample of receptor medium was withdrawn at predetermined time points and replaced with fresh medium. At the end of the experiment, the residual formulation in the donor compartment was carefully rinsed with PBS and quantitatively collected. The amount of CqP accumulated inside the membrane was determined by finely chopping the tissue with a scalpel and homogenizing it with a pestle in PBS first, then in acetonitrile to disrupt cell membranes. The homogenates were centrifuged (10,000 rpm, 10 min) and the supernatant diluted with mobile phase prior to injection in HPLC. The validated HPLC–UV method described in Sect."Analytical method for chloroquine diphosphate assay", was used to quantify the amount of drug permeated. A drug mass balance higher than 90%, *i.e.*, the sum of the amounts of CqP recovered from the two compartments plus the mucosa, was assessed.

From the amount of CqP extracted from the mucosa, the concentration of drug accumulated within the membrane was then determined, by calculating the membrane volume as cylindrical slab geometry from area (0.58 cm^2) and thickness (average thickness of rabbit nasal septum mucosa: 167 µm according to [26]).

Time lag and drug flux were determined from the slope of the linear portion of permeation profiles. Experiments were replicated at least three times. A chloroquine diphosphate solution in water (7.5 mg/ml), loaded at the same drug dose (7.5 mg), was tested as reference.

In vitro antiviral activity of the spray-dried nasal powders on Vero E6 cells infected with SARS-CoV-2

SARS-CoV-2 was isolated from RT-PCR positive patients and propagated in cell cultures of Vero E6 cells (ATCC CRL-1586), a continuous line isolated from African green monkey (formerly known as *Cercopithecus aethiops*) kidney epithelium. Vero E6 cells were maintained in Eagle's medium (EMEM) supplemented with 10% heat-inactivated fetal bovine serum (FBS), 1% penicillin–streptomycin (P/S) and 1% L-glutamine (L-Gln). These cells were infected with SARS-CoV-2 and treated with the antiviral powders to measure their antiviral effect. For the purpose, either chloroquine diphosphate monocomponent or the binary (with zinc gluconate) or ternary composite (with zinc gluconate and lactoferrin) spray-dried powders were dissolved in EMEM to reach the final concentration of 10 mM of chloroquine diphosphate (stock solutions). Each stock was then diluted to make the actual test solutions.

Vero E6 cells were seeded in 96-wells plates at a density of 2.5×10^4 cells per well and grown for 24 h at 37 °C in CO_2-enriched atmosphere. Cytotoxicity on Vero E6 cells of drug concentrations of 25, 50, 75 and 100 µM, was determined by staining cells with a 4% formaldehyde solution in Crystal violet to detect the viable ones.

In the evaluation of the antiviral activity, only the three lowest CqP concentrations were tested. As for the SARS-CoV-2 viral load to infect Vero E6 cells, in a series of preliminary experiments, four levels of multiplicity of infection (MOI) were considered, *i.e.*, 0.005, 0.05, 0.2 and 0.8. The MOI is the ratio between the number of virions inoculated and number of cells in culture. Cell contact with the virus lasted 1 h at 37 °C. Later, the main experiments were performed only at the two lowest MOIs (0.005 and 0.05), as they are near the median viral titer of an infected subject [27–29].

In the main experiments, the antiviral activity of the formulations was tested according to four protocols:

A. Vero E6 cell infection followed by one drug treatment;
B. Vero E6 cell infection followed by three drug treatments;
C. Vero E6 cell pre-treatment with drug followed by virus inoculum (infection) and one drug treatment post-infection;
D. Vero E6 cell pre-treatment followed by infection and three drug treatments post-infection.

In experiment A, Vero E6 cell cultures were infected with viral solutions at the desired MOI and incubated for 1 h. Then, drug-free medium was added and incubation continued for 3 h. After incubation, the drug solution was added to the infected cell cultures for the 2-h drug treatment. At the

end, cells were washed and incubated with drug-free fresh medium for 48 h.

In experiment B, Vero E6 cells were infected as described for protocol A. After infection and subsequent incubation, the cell culture was treated with the drug three times; every treatment lasted 2 h and was followed by a 3-h incubation with drug-free fresh medium.

For experimental protocol C, Vero E6 cells were pre-treated for 2 h with 100 µl of drug powder solution at the CqP test concentration (25–50-75 µM), and then washed with EMEM. 100 µl of virus was then added to infect the cell culture at the predefined MOI. After 1-h contact with the virus, 100 µl of drug-free fresh medium was added and cells were incubated for 3 h. Next, the drug solution at the desired test concentration was added to treat the infected cell cultures for 2 h. At the end, cells were washed and incubated with fresh drug-free medium for 48 h.

In experiment D, Vero cell cultures were pre-treated as in protocol C and then incubated for 1 h with the virus (infection). After incubation, the cell culture was treated with the drug three times: every treatment lasted 2 h and was followed by a 3-h incubation with drug-free fresh medium.

In all experiments, 10 µl of the supernatant from each replicate was collected and pooled after the last addition of fresh medium, and after 24 and 48 h of incubation. Viral RNA was quantified by qRT-PCR using Allplex Seegene Extraction Free protocol.

For executing the preliminary experiments with 4 MOIs and 3 drug test concentrations, the 96-well plate was organized as follows: for each drug concentration 4 columns were used, one per MOI, thus obtaining seven replicates (7 wells) for each viral MOI/CqP concentration combination. The last row was for virus control wells, cytotoxicity control wells, and cell control wells.

For the main experiments at two MOIs, the 96-well plate was organized to have 14 replicates for every viral MOI/CqP concentration combination. The last row was used for the controls.

Data analysis for antiviral activity The adopted semi-quantitative method to detect viral nucleic acid (quantitative reverse transcription polymerase chain reaction, qRT-PCR), led to a cycle threshold value (Ct) for each treatment and for the untreated virus control. Three viral genes were detected, namely *E* gene, *RdRp/S* gene e *N* gene, but only Ct values for the *N* gene were used for analysis. *N* gene is the most common target for detecting SARS-CoV-2. Recently, the attention has turned on the genetic variability and evolution of *N* gene, which may affect reliable detection [30]. Thus, each experiment generated the following raw data:

- Ct value at time 0 h, *i.e.*, before drug treatment (the value was the same for virus control and each treatment group);
- Ct value at time 48 h, *i.e.*, after drug treatment (the values were different for the untreated virus control and each treatment group).

Ct value is inversely proportional to the magnitude of viral load, but represents a theoretical measure of the quantity of viral genome because qRT-PCR analysis is semiquantitative [31]. Nevertheless, the reduction of Ct value from 0 to 48 h indicates that the viral load has increased, *i.e.*, the virus has replicated in the cells. Brandolini et al. demonstrated a correlation between Ct values and the number of RNA copies per µl, which are obtained by quantitative digital polymerase chain reaction (dPCR) analysis [31]. Therefore, the number of RNA copies per µl was calculated from Ct values for both controls and treatments to provide a better quantification of the viral load before and after treatment.

Then, the treatment effect on viral replication was expressed as the difference between the $\log_{10}$ of the number of RNA copies per µl at 48 h and at time 0 h, according to the following formula:

$$\Delta\log_{10}(\text{RNA copies}/\mu l) = \log_{10}(\text{RNA copies}/\mu l)_{48h} - \log_{10}(\text{RNA copies}/\mu l)_{0h}$$

The same difference was calculated for the virus control and then used to calculate the % inhibition by the treatment *vs.* the untreated control according to Eq. 2:

$$\%inhibition = \left[1 - \left(\frac{\Delta log10(n.\text{RNA copies}/\mu l)_{TREATMENT}}{\Delta log10(n.\text{RNA copies}/\mu l)_{\text{VIRUS CONTROL}}}\right)\right] \times 100 \quad (2)$$

Statistical Analysis

The data were compared by an unpaired two-tailed Student's t-test. p values less than 0.05 were considered to indicate statistical significance.

Results and discussion

Viral airborne diseases mostly proceed by inhalation of infectious microdroplets dispersed in the air. Nose, throat, pharynx and larynx are the first sites of virus deposition and infection, as witnessed by the anosmia and dysgeusia occurring in COVID-19. Hence, the antiviral treatment should be timely applied first in the upper airways for a loco-regional therapeutic action [32, 33].

The nasal powders of this study contained chloroquine diphosphate (CqP) that demonstrated activity on coronaviruses like SARS-CoV-2 [15, 17, 34]. We deemed to repurpose this drug as the first candidate for the preparation of novel antiviral nasal powders. CqP was preferred to hydroxychloroquine for the nasal application because of its lower polarity easing permeation across cell membranes [35].

The clinical unsuccess of systemic antiviral drugs in COVID-19 was likely related to the fact of not reaching effective concentrations in the infected epithelial cells despite the high doses administered. The daily oral dosages of nirmatrelvir/ritonavir combination or the single drug molnupiravir were in the order of hundreds of milligrams to attain active concentrations at target infected tissue [36, 37]. Delivering the drug directly onto the upper airway cells opens the possibility to increase intracellular antiviral concentrations at much lower administered doses. We selected a nasal unit dose of CqP of 25 mg, *i.e.*, 1/10 of the minimum oral unit dose proposed for vulnerable and elderly patients [19].

Table 2 Moisture content and particle size distribution data (d_v, volume diameter; the subscript number indicates the percentile of the cumulative undersize distribution) of the three CqP nasal powders (mean ± SD; n = 3)

Formulation	Residual moisture (%w/w)	$d_{v,10}$ (μm)	$d_{v,50}$ (μm)	$d_{v,90}$ (μm)
CqP monocomponent	1.9 ± 0.1	1.2 ± 0.0	3.7 ± 0.5	7.8 ± 0.1
CqP binary composite	1.8 ± 0.1	1.3 ± 0.1	4.7 ± 0.3	10.7 ± 0.6
CqP ternary composite	2.5 ± 0.2	1.9 ± 0.5	4.5 ± 0.5	9.3 ± 0.8

Microparticulate nasal powders of chloroquine diphosphate compositions can be manufactured by spray drying

The spray drying conditions applied for manufacturing the nasal powders enabled to obtain engineered particles in the micrometer size range from aqueous solutions of combined antiviral agent and excipients. In fact, a CqP monocomponent spray-dried powder, a binary composite powder of CqP and zinc gluconate and a ternary composite powder of CqP, zinc gluconate and lactoferrin were prepared (Table 1). Production yields were always > 80% despite the small batch size processed. About 2% (w/w) of moisture remained as residue in the powders (Table 2). Chloroquine diphosphate assay of the nasal powders confirmed the expected drug content, which remained stable during the investigation.

The binary and ternary compositions were formulated to enhance the antiviral activity of the particles on the upper airway epithelia. In particular, the addition of zinc gluconate was motivated by the evidence that chloroquine acts as a zinc ionophore, facilitating the entry of Zn^{2+} ions into cells, where this microelement contributes to the inhibition of virus replication [38]. Lactoferrin in the ternary composite intended to improve the bio-adhesivity of the nasal powder, owing to the lactoferrin-enriched surface of these microparticles created during droplet spray drying [39]. Moreover, the protein isoelectric point of 8–9 makes it positively charged at the slightly acidic pH of nasal cavity [40, 41]. Electrostatic interactions with the negatively charged mucus glycoproteins can mediate the bioadhesion [42, 43]. Further value of the use of lactoferrin in the ternary composite is its antiviral activity against several viruses, including SARS-CoV-2 [44–46].

After manufacturing, the three CqP microparticulate powders were characterized in view of their administration to the upper airways by a nasal sharp sniff, aiming to prompt a loco-regional antiviral action. Their high CqP concentration was suitable to load powder amounts equivalent to the 25 mg CqP unit dose into the size #3 hard capsules used as powder reservoir in the Turbospin® device.

The micromeritics of CqP spray-dried powders suits broad deposition in the nasal cavities and upper airways

In view of their deposition onto the upper airways, the aerodynamics of CqP microparticles aerosolized by nasal inspiration through the Turbospin® device, requires particle properties tuned to the low airflow rate generated. Geometric and aerodynamic size distributions, shape, bulk density, and flowability were the tested properties of spray-dried

microparticulate powders. Table 2 reports the size distributions in volume diameter of the three formulations.

The median volume diameter of the spray-dried particles ($d_{v,50}$) was lower than 5 μm for all formulations. According to the Ph. Eur. monograph of nasal powders, "the size of particles is such that their deposition is localized in the nasal cavity". Consequently, if the target region was the nasal cavity only, 10 μm would be the lower limit for the size of nasal powder particles [47, 48]. Here though, all powders had geometric particle size distributions with 90% of particles smaller than 11 μm, which meet our goal of delivering CqP across and beyond the nasal cavity. Such fine particle size determines a large specific surface area to coat the upper airways by the aerosol peculiarly generated by a nasal inhalation act. Several studies have indicated that SARS-CoV-2 has the nose and upper airways as the first sites for replication and spreading [49, 50]. By intaking the nasal powder via a nasal sharp sniff, the antiviral particles aerosolize and travel the same route of the infectious viral droplets. Therefore, the prepared spray-dried nasal powders benefit from their very fine size distributions, the goal being an antiviral loco-regional targeted intervention at the early infection symptoms. In addition, depending on the medical prescription, the prepared nasal powders have the size to be also possibly aerosolized by oral inhalation directly into the lungs.

The micromeritics characteristics of the nasal powders relevant to both capsule filling and aerosol formation, were determined (Table 3).

The spray-dried powders exhibited low untapped bulk density, favorable for aerosol formation and emission from the powder-loaded capsule. Calculated Carr indexes classified the powders as very poorly flowable, at the bottom of the scale of flowability [51]. The measured dynamic angles of repose in the range 43–50°, correlated well with the Carr index, indicating a certain cohesiveness of the three nasal powders [52]. Anyway, the properties of the three powders were equivalent with respect to powder metering and aerosolizing.

The shape of particles for inhalation is another relevant feature for the aerodynamic performance of the powder. The CqP monocomponent particles had spherical shape and perfectly smooth surface (Fig. 3A). The degree of smoothness slightly changed in the larger particles (> 2 μm) as small dimples appeared on the surface.

Table 3 Untapped and tapped bulk densities, Carr index, and dynamic repose angle of the CqP nasal powders (mean ± SD; n = 3)

Formulation	Untapped bulk density (g/ml)	Tapped bulk density (g/ml)	Carr Index (%)	Dynamic repose angle Φ
CqP monocomponent	0.25 ± 0.01	0.40 ± 0.01	37 ± 0.3	50.1 ± 1.3
CqP binary composite	0.17 ± 0.01	0.27 ± 0.01	36 ± 0.3	42.7 ± 0.4
CqP ternary composite	0.23 ± 0.01	0.38 ± 0.01	38 ± 0.8	47.6 ± 1.8

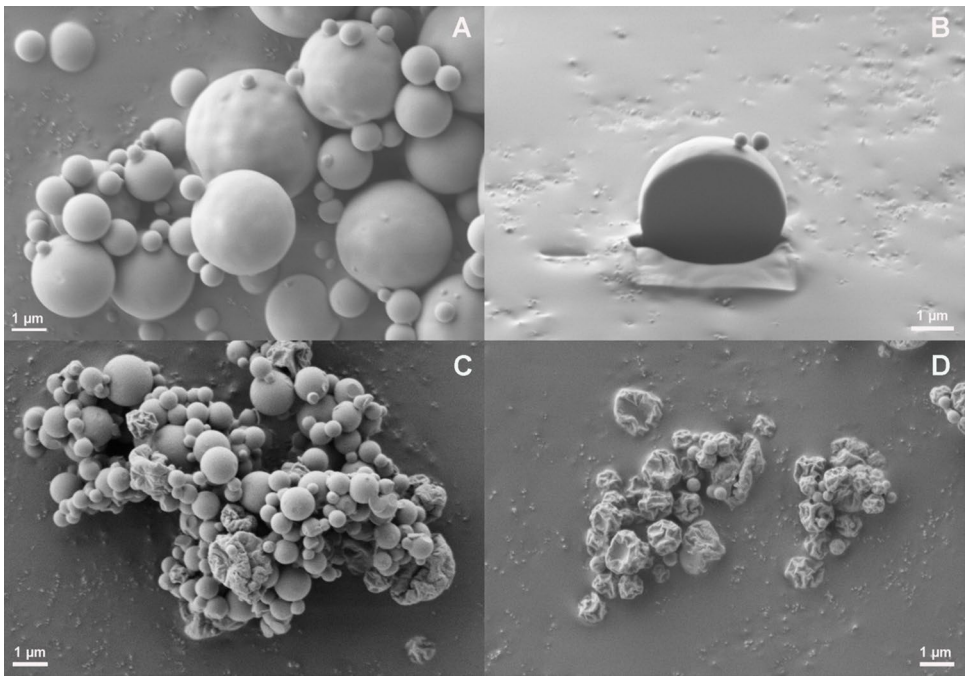

Fig. 3 FESEM micrographs of the spray-dried nasal powders. **A**) CqP monocomponent; **B**) FESEM-FIB image of the internal structure of a CqP monocomponent microparticle; **C**) CqP binary composite; **D**) CqP ternary composite. The magnification was 20 KX in all cases, except for the single microparticle where it was 25 KX (image B)

In addition, the inner part of these particles was fully dense, as revealed by the SEM image of a single microparticle FIB-cut cross-section acquired in tilted conditions (Fig. 3B). The darker area is actually the internal section of the particle. Finally, the individual particles did not show interparticle bridges.

The addition of 20% of zinc gluconate to the CqP aqueous solution to spray dry affected the formation of the largest spherical particles during droplet drying and solidification. In fact, the crust of the solid surface in formation did not mechanically resist the sphere curvature. Consequently, the largest particles collapsed [53]. The result of this behavior was that several corrugated particles were present in the quite small CqP binary composite population (Fig. 3C). Comparing the particle populations of Fig. 3C and 3 A, one notices that the largest particles disappeared because they selectively collapsed; only the smaller particles resisted to the tension of the dry spherical geometry.

The ternary composite microparticles had the typical wrinkled morphology of spray-dried particles of proteins (Fig. 3D). Having lactoferrin a higher molecular weight than chloroquine diphosphate and zinc gluconate, it diffuses more slowly during droplet drying and concentrates at the surface of droplet, determining the crumpled aspect of dry particles.

According to the FESEM micrographs, the CqP monocomponent microparticles (Fig. 3A) appear larger than those containing the excipients (Fig. 3C-D), thus not matching the size distributions obtained by laser diffraction (LD) (Table 2). On one hand, this contradictory result may be due to few particle aggregates in the liquid samples for LD analysis, which were not fully dispersed despite the surfactant presence. However, it should be underlined that the size distribution by LD is obtained from the analysis of a statistically significant number of particles in the sample, whereas the SEM micrographs of a small group of discrete particles may be less representative of the actual distribution. Anyhow, the size of all three spray-dried nasal powders was similar and suitable for their deposition onto the upper airways.

Finally, X-ray diffractograms and DSC scans of the three spray-dried powders showed the amorphous state of chloroquine diphosphate and its full miscibility with the excipients (Supplementary Material, Fig. S1-S2).

The nasal inspiration (sharp sniff) airflow enabled powder dose extraction from the device by healthy volunteers

Since nasal powders are combination products, in this study the antiviral microparticulate formulations were combined with the commercially available dry powder inhaler (DPI) Turbospin® (Fig. 2). It is a pre-metered passive device used for oral inhalation of powders. In the present application for nasal delivery, it was employed performing a nasal

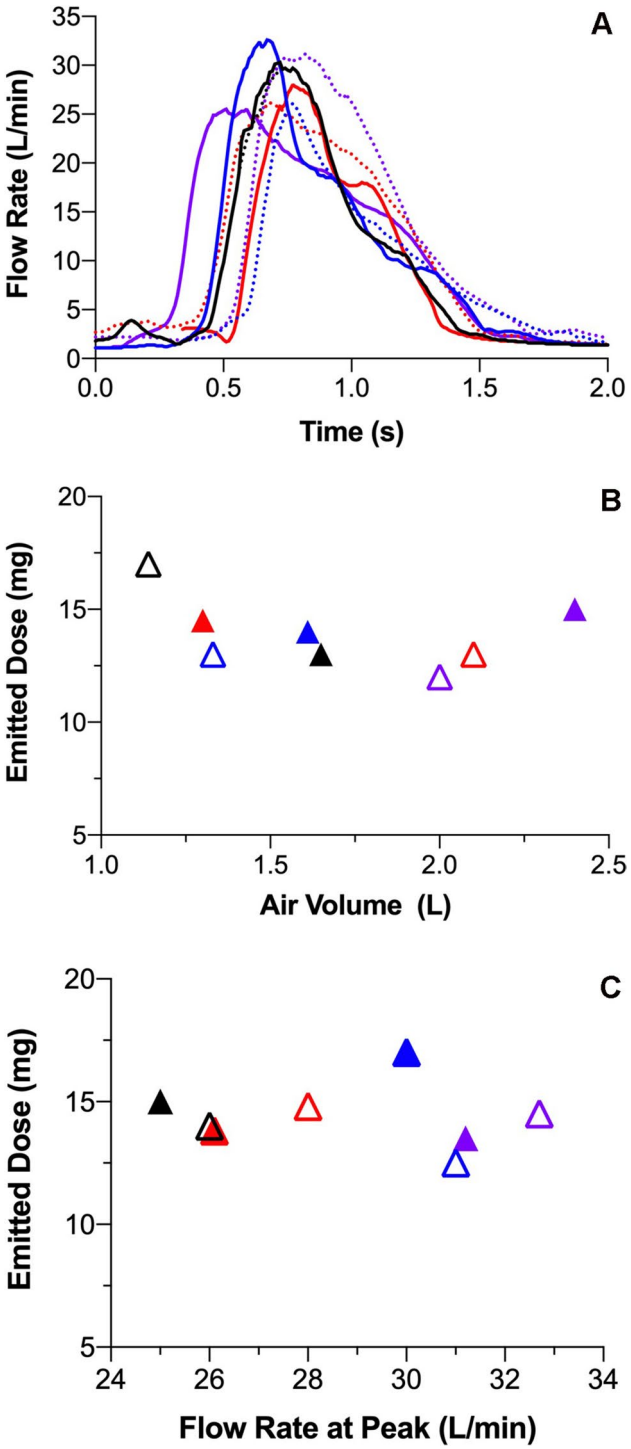

Fig. 4 Airflow dynamics and powder emission upon nasal inhalation through the Turbospin® DPI by four human volunteers (each one identified by the line/symbol color). **A**) Individual airflow patterns of two consecutive nasal sniffs through the device (1st sniff: continuous line; 2nd sniff: dotted line); **B**) Relationship between the emitted powder dose with each sniff and the inhaled air volume (1st sniff: filled symbol; 2nd sniff: empty symbol) **C**) Relationship between the emitted powder dose with each sniff and the airflow rate at peak (1st sniff: filled symbol; 2nd sniff: empty symbol). The device was loaded with a size #3 HPMC capsule containing 35.7 mg of a spray-dried mannitol powder, manufactured according to Quarta et al. [22]

inhalation act through the nostril. In fact, the shape and size of its mouthpiece allow for its insertion into the nostril. Indeed, the nasal use of a device originally designed for oral lung inhalation, accomplished the novel delivery concept of this research, *i.e.*, to extract the antiviral powder with the nasal airflow and target aerosol deposition onto the upper airways. The maneuver can be repeated alternating the nostrils until the capsule is completely emptied.

The airflow rate generated through the device by a nasal inhalation act of a spray-dried mannitol powder [22] was measured in healthy volunteers. Four subjects performed two nasal sharp sniffs, one per nostril, through the device loaded with a hard capsule containing about 35 mg of the mannitol powder. The airflow rate values measured during each inhalation varied among the subjects, reaching the flow rate peak of inhalation between 25–35 L/min. The inspiration lasted about 1 s (Fig. 4A). The mass of powder emitted per sniff ranged between 13 and 18 mg (Fig. 4B).

The emitted dose did not correlate with the air volume drawn through the device, which ranged between 1.0 and 2.5 L (Fig. 4B). There was also no relationship between the emitted dose and the peak of the airflow (Fig. 4C). It is noteworthy that the same ramp-up of the nasal inhalation flow rate curves was recorded, which is considered the determining parameter for powder extraction from DPIs [54, 55].

Notably, all volunteers reported an almost immediate perception of a slightly sweet fresh taste in the throat (oropharynx) that qualitatively proved the loco-regional deposition and dissolution of the mannitol particles. Thus, the emitted aerosol moving inside the nose passage, reached the upper airway surface and provided an intimate contact between powder and epithelial cells.

The nasal inhalation airflow rate increased the MMAD for effective deposition onto the upper airways

Spray-dried powders engineered for lung deposition, aerosolized at airflow rates between 25–35 L/min, could be inhaled through the nose with the Turbospin® device for loco-regional deposition of CqP in the infected upper airways. The inhalation act through the nose generates a significantly lower airflow rate than the oral act [23]. Nevertheless, the fraction of mannitol powder extracted per single sniff by the volunteers ranged between 35 and 50% of the amount loaded in the capsule.

In inhalation, the aerodynamic behavior of the powder particles to aerosolize by an inhaler, is the critical quality attribute to study in dependence on the airflow rate. It affects the probability and region of particle deposition [56]. Thus, the aerodynamics of the dispersion and deposition of the three CqP formulations was assessed using the Next Generation Impactor (NGI) to measure the aerodynamic diameter distribution of the aerosol particles produced in conditions of nasal or oral inhalation through the Turbospin®. The measurements were first conducted under the provisions of lung DPI testing at 4 kPa of pressure drop, corresponding to mouth flow rates of 65 L/min (4 L of air passing through), and then at 1 kPa of pressure drop, corresponding to the nasal airflow rate of 34 L/min measured in vivo (4 L) (see Fig. 4A). Being aware that the NGI configuration does not reproduce the structure of the upper airway passage, the test was carried out aiming to assess the aerodynamic quality of the product extracted by nasal inspiration. Table 4 shows the emission values of the three formulations aerosolized through the Turbospin® at the two pressure drop values corresponding to the airflow rates of nasal and oral inhalation, respectively.

Table 4 Aerodynamic parameters of CqP spray-dried nasal powders aerosolized by Turbospin® at 4 kPa (airflow rate 65 L/min; volume 4 L) and 1 kPa (airflow rate 34 L/min; volume 4 L). The values were obtained using the NGI apparatus (mean ± SD; n ≥ 3). The metered CqP dose in the capsule was 25 mg for all powders, corresponding to different loaded amounts for each powder based on its composition (Table 1)

Formulation	Powder loaded (mg)	Pressure Drop (kPa)	CqP Emitted Dose (mg)	CqP Fine Particle Dose (mg)	MMAD[a] (μm)	GSD[b]
CqP monocomponent	25.5	4	20.1 ± 0.1	5.2 ± 0.1	6.80 ± 0.05	1.83 ± 0.02
		1	16.7 ± 0.3	3.3 ± 0.1	7.8 ± 0.1	2.60 ± 0.01
CqP binary composite	31.3	4	21.1 ± 0.2	3.8 ± 0.2	7.40 ± 0.02	1.90 ± 0.03
		1	18.1 ± 0.2	3.1 ± 0.2	8.1 ± 0.1	2.50 ± 0.02
CqP ternary composite	35.7	4	20.4 ± 0.1	6.3 ± 0.2	5.8 ± 0.1	2.60 ± 0.01
		1	19.8 ± 0.2	3.9 ± 0.2	7.6 ± 0.1	2.50 ± 0.02

[a]Mass Median Aerodynamic Diameter

[b]Geometric Standard Deviation

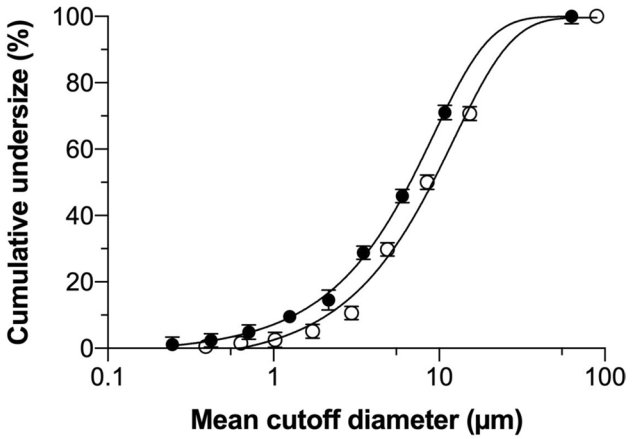

Fig. 5 Aerodynamic particle size distributions of CqP ternary composite at 1 kPa (white circle) and 4 kPa (black circle) pressure drop, respectively corresponding to nasal and oral airflow rate (mean ± SD; n = 3). The last point of each curve, corresponding to the fraction deposited in the NGI induction port, was arbitrarily assigned to a size value estimated based on a $2\sqrt{2}$ progression of the size. The lines are the fitting of the experimental data with a non-linear regression model (Prism 9.0; GraphPad Software, Boston, MA, USA)

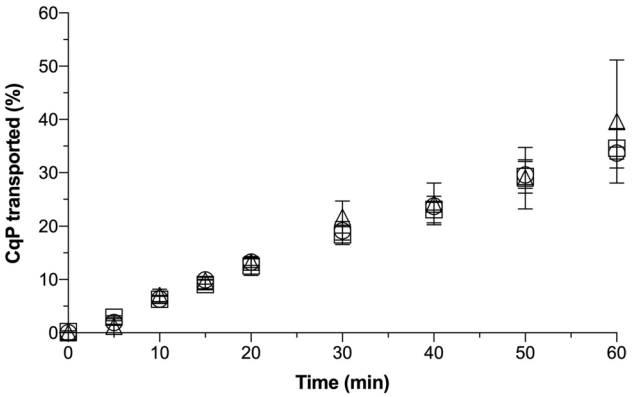

Fig. 6 In vitro dissolution of CqP and diffusive transport across a regenerated cellulose membrane from spray-dried microparticles of CqP monocomponent (circle); CqP/zinc gluconate binary composite (square); CqP/zinc gluconate/lactoferrin ternary composite (triangle) (mean ± SD; n ≥ 3)

From the aerodynamic assessment at 65 L/min (4 kPa pressure drop), the CqP emitted fractions for the three powders were > 80% in all cases. Most of the powder mass that escaped the NGI induction port was deposited on the impactor first stages, leading to CqP fine particle doses between 3.8 and 6.3 mg and an MMAD (Mass Median Aerodynamic Diameter) in the range 5.8—7.4 µm.

Conversely, when the same powders were extracted at the lower airflow rate corresponding to 1 kPa pressure drop, both the CqP monocomponent and binary composite had an emitted dose lower than 75%. The fine particle dose, *i.e.*, the dose of microparticulate powder with an aerodynamic size of less than 5 µm, decreased of about 8–38% upon reduction of the inhalation airflow rate. The most efficient formulation, in terms of aerosolization and deposition at the nasal airflow rate, was the CqP ternary composite. Figure 5 shows the aerodynamic particle size distributions of this composite at the two airflow rates considered. The cumulative undersize curves show a significant shift towards higher sizes when the airflow rate was reduced to simulate the conditions of the nasal inhalation act.

Translating these data to the envisaged upper airway deposition upon nasal sniff, it is encouraging that the MMAD of the nasal aerosol significantly increased by 1.3 folds at 34 L/min. In fact, this limits the deposition of fine particles into the deep lung. At the same time, fractions of fine particles will travel beyond the nasal cavity for a deposition onto the oropharynx and larynx, coating a large surface where intracellular absorption will take place. In vitro deposition studies with the CqP monocomponent nasal powder in the Alberta Idealized Nasal Inlet coupled with NGI, are currently ongoing. Ninety percent of powder deposition was measured from nostril to NGI Stage 1 (10.95 µm cut-off at 34 L/min) that represent the upper airways, with only 4.5% of respirable fraction (preliminary data). The chance that this small fraction of the nasal aerosol reaches the lungs must not be considered a drawback in the loco-regional therapy of viral infections. In fact, the concept of an orally inhaled antiviral therapy to ensure higher drug concentration in the infection site, was considered during the COVID-19 pandemic [57, 58]. However, pulmonary administration disregarded that in the early phase, the infection involves mainly the upper airway epithelia. In particular, hydroxychloroquine was administered to the lung of healthy volunteers by oral inhalation and proved safe and well tolerated [59].

The in vitro dissolution of chloroquine diphosphate nasal powders was fast

The dissolution rate of powder formulations deposited on the nasal mucosa is a crucial step for intracellular local absorption of the antiviral drug administered by a nasal sharp sniff. The dissolution and diffusive transport of CqP from the three spray-dried microparticulate powders deposited on a non-partitioning membrane on Franz-type cells, is shown in Fig. 6.

The CqP transport through the artificial membrane was quasi linear during the first 30 min. Visually, it was observed that the disappearance of CqP powders on the membrane was accomplished in about 20 min, independently of the powder composition. The linearity of the dissolution profiles of all formulations in the early time, suggests that pseudo-steady state conditions were quickly established,

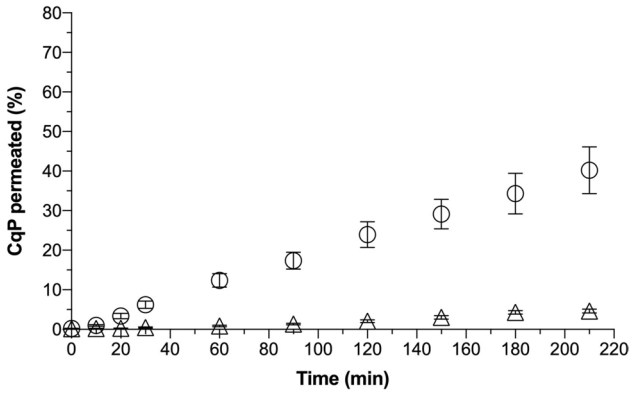

Fig. 7 Percent of CqP permeated ex vivo across rabbit nasal mucosa from 7.5 mg of raw material powder wet with 0.1 ml of PBS pH 7.4 (circle) and 1 ml of a 7.5 mg/ml CqP solution in water (triangle) (mean ± SEM; n ≥ 6)

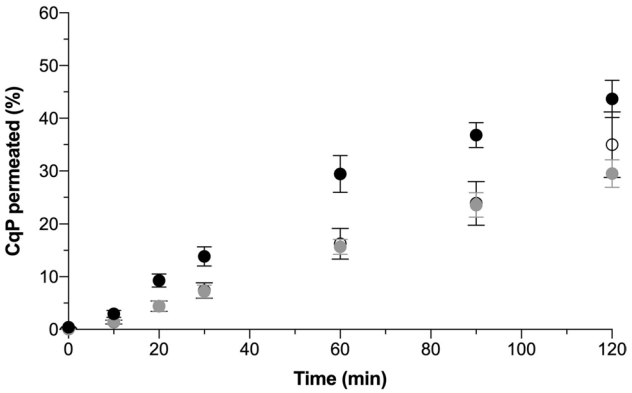

Fig. 8 Percent of CqP permeated ex vivo across rabbit nasal mucosa from 7.5 mg of CqP as spray-dried monocomponent (black), CqP/zinc gluconate binary composite (grey) and CqP/zinc gluconate/lactoferrin ternary composite (white) microparticles (mean ± SEM; n ≥ 6)

with negligible time lag, until 30 min. This implies that, in the applied experimental conditions, the powder dissolved quickly and formed a solution with a constant CqP concentration in the donor. The reported equilibrium solubility of CqP in water is 0.25 g/g at 35 °C [60]. Here, having 10 mg CqP and 0.1 ml of solvent in the donor, the CqP solutions formed on the membrane were reasonably saturated in the early time of transport.

The three superimposed dissolution profiles suggest that neither zinc gluconate nor lactoferrin affected the drug dissolution rate in the applied experimental conditions. After 30 min, the linear transport profiles curved down, signaling the decrease of dissolved drug concentration in the donor.

Referring to the paper of Frenning and co-workers [61] on modelling of the dissolution rate of a powder deposited on a permeable membrane, here the ratio between dissolution time and diffusion time in the performed experiments should be around 1. It means that the particle dissolution rate does not represent a limiting factor for the drug diffusive transport through the membrane.

Chloroquine diphosphate extensively permeated from the powders across the nasal mucosa and accumulated at mM concentrations

Ex vivo permeation studies with the rabbit nasal mucosa allowed to assess the antiviral drug transport from deposited nasal powders. Drug permeation rate and accumulation within the mucosa *vs.* contact time were determined as influential parameters for the antiviral action in the upper airways. The profiles in Fig. 7 compare the drug permeation respectively from 7.5 mg of chloroquine diphosphate raw material and from 1 ml of a 7.5 mg/ml CqP solution in water. We used unprocessed CqP raw material here instead of the CqP monocomponent spray-dried powder to avoid any effect on permeation by the powder solid state as determined by the spray drying process.

The rate of drug permeation from CqP raw material powder dissolving in 0.1 ml of phosphate buffered saline, approximated pseudo-steady state conditions from 10 to 60 min, at a flux of 28.4 ± 3.6 μg cm^{-2} min^{-1}. In the same interval, the flux from the CqP solution was 1.8 ± 0.4 μg cm^{-2} min^{-1}. At 210 min about 5% of CqP, loaded as solution, had diffused through the membrane. Conversely, in the same 3 h period 40% of the CqP deposited as raw material particles, was transported (Fig. 7). This eightfold difference was due to the tenfold difference in CqP concentrations in the donor.

The ex vivo CqP permeation across the rabbit nasal mucosa from the spray-dried formulations was subsequently tested. The comparative permeation profiles aimed at assessing the influence of the composition of the spray-dried particles on CqP transported. For consistency with the CqP dose of the previous experiment, 7.5 mg of CqP as monocomponent, binary or ternary composite particles were spread onto the partitioning membrane. As before, the powder was wet with 0.1 ml of PBS pH 7.4. Figure 8 shows the three permeation profiles of CqP obtained.

After a short time-lag, the permeation proceeded at a substantially constant rate until 60 min for the three formulations, revealing pseudo-steady state conditions of diffusion. The CqP permeation flux from the monocomponent spray-dried microparticles in this time interval was 66.8 ± 8.6 μg cm^{-2} min^{-1}, faster than the binary composite (45.4 ± 3.6 μg cm^{-2} min^{-1}; $p = 0.04$), and the ternary (44.1 ± 7.5 μg cm^{-2} min^{-1}; $p = 0.06$). Therefore, zinc and lactoferrin components in the spray-dried composite powders slowed down the permeation flux of CqP through the biological barrier. This composition-related difference had not been observed during the dissolution and transport of chloroquine across the non-partitioning cellulose membrane,

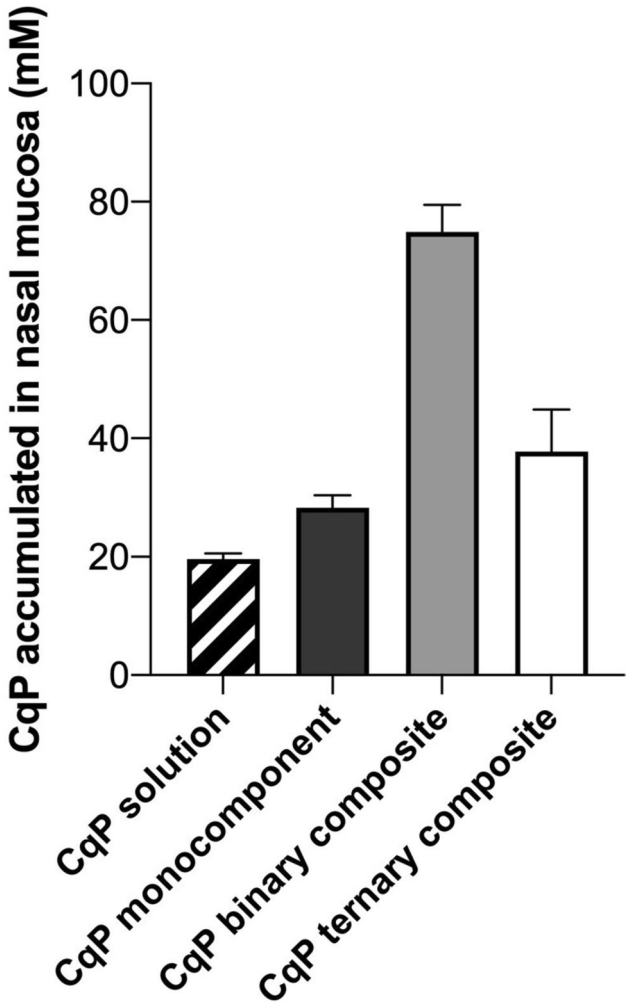

Fig. 9 Concentration (mM) of chloroquine diphosphate in rabbit nasal mucosa after 210 min of permeation experiments. Donor: 1 ml of 7.5 mg/ml CqP solution in water (black and white), CqP monocomponent (black), CqP binary (grey) and ternary composites (white) (mean ± SEM; n ≥ 6)

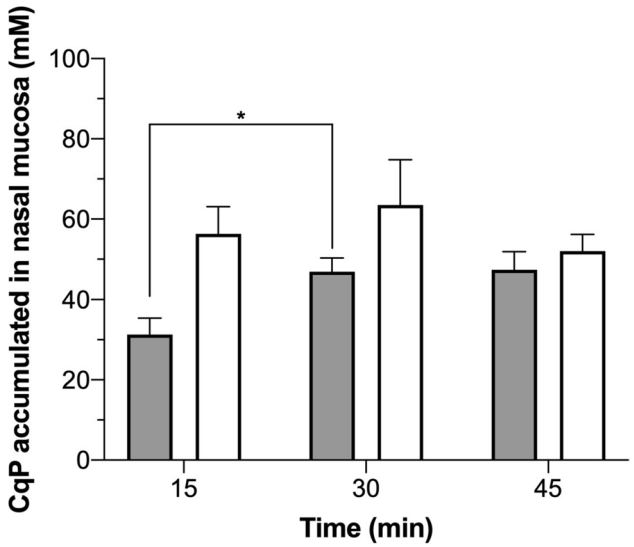

Fig. 10 Concentrations (mM) of chloroquine diphosphate in the rabbit nasal mucosa after 15, 30 and 45 min of contact with CqP binary composite (grey) and CqP ternary composite (white) (mean ± SEM; n ≥ 3). The asterisk indicates statistical significance ($p < 0.05$)

where the three nasal powders exhibited superimposed profiles. In contrast, in the biological partitioning membrane, the concomitant presence of Zn^{2+} and lactoferrin had a negative influence on CqP transport across the rabbit nasal tissue.

We have just showed in Fig. 7 that the permeation of CqP across the rabbit nasal mucosa benefited from the "locally dissolving powder effect". The results with the spray-dried formulations confirm that a CqP nasal powder deposited on the nasal epithelium is an effective strategy for improving drug transport [62]. Notably, the ex vivo CqP permeation from the monocomponent powder outperformed the raw material (Fig. 7), confirming that spray drying modified particle properties in the solid state, in a way impacting on drug dissolution and permeation. The CqP monocomponent powder was indeed amorphous, while the raw material was crystalline (Fig. S2-S3).

At the end of permeation experiments with spray-dried powders (210 min), chloroquine diphosphate inside the mucosa membrane was extracted and quantified to calculate its concentration in mM units (Fig. 9). This represents the intraepithelial drug concentration that expectedly provides the antiviral activity towards infected cells.

Following the 210 min transport from the CqP solution and CqP spray-dried monocomponent powder, drug concentration inside the tissue was 14.4 ± 3.1 mM (0.8% of CqP loaded amount) and 28.3 ± 2.1 mM (1.7% of CqP loaded amount), respectively (Fig. 9). Such values must be considered active concentrations, according to reported in vitro IC_{50} of 0.005 mM for CqP [63]. The CqP spray-dried monocomponent powder accumulated a concentration of drug lower than the binary and ternary composite powders within the nasal mucosa, that reached 80.1 ± 6.5 mM and 37.7 ± 7.1 mM, respectively (Fig. 9). It is strikingly interesting to note that the concentration of CqP in the membrane was very high when zinc gluconate was the only additive in the powder composition. Zn^{2+} ions were present also in the ternary composite together with lactoferrin. Their concurrent presence in the ternary powder slightly improved the tissue drug accumulation compared to the CqP monocomponent powder ($p = 0.23$). These results suggest that zinc ions promoted chloroquine diphosphate accumulation into the epithelial cells during the permeation experiment. This effect could be related to the fact that chloroquine is a Zn^{2+} ionophore that forms lipophilic complexes with the metal [38, 64]. In the case of the ternary powder, the lower membrane

accumulation can derive from lactoferrin disturbing the interaction between zinc ions and chloroquine, since lactoferrin protein binds divalent cations [65].

In summary, at the end of the permeation experiments with the spray-dried microparticles, greater amounts of CqP had accumulated in the tissue in presence of zinc. Indeed, with the binary composite, 0.38 ± 0.03 mg (4% of CqP loaded dose) of CqP were quantified in rabbit nasal epithelium. Thus, 14–80 mM concentrations of chloroquine diphosphate were established in the rabbit nasal mucosa, *i.e.*, more than three orders of magnitude the antiviral concentration reported in the literature [63]. The permeability of CqP favors the nasal tissue accumulation upon deposition of the powder. Accordingly, the logP of 4.63 classifies chloroquine free base as highly lipophilic drug.

As the mucociliary clearance quickly removes material deposited onto the nasal mucosa, shorter contact times between powder formulation and mucosa have been investigated for the binary and ternary composites (15, 30, 45 min). Interestingly, after 15 min, the CqP concentration within the mucosa was about 30 mM for the binary composite and almost 60 mM for the ternary composite (Fig. 10).

Such rapid achievement of these intraepithelial antiviral concentrations significantly increased with contact time for the binary composite before stabilizing for both compositions after 30 min. As previously observed, in 210 min of contact, the binary composite accumulated about 1.7 folds more CqP than the ternary composite (Fig. 9).

This rapid accumulation of CqP after a short contact time with the nasal mucosa is encouraging for the locoregional antiviral therapy. When the nasal inspiration is successful in depositing the powder in the upper airways, an active intraepithelial concentration would be rapidly achieved.

The nasal powders showed anti-SARS-CoV-2 activity in vitro

Microbiological studies allowed to determine the antiviral activity of the spray-dried nasal powders against SARS-CoV-2-infected cells. It is widely documented that Vero E6 cells are sensitive and permissive to SARS-CoV-2 infection, leading to high titer replication of virus [66]. The attention here was directed to the activity of the composite powders, because the combination of chloroquine diphosphate, zinc gluconate and lactoferrin had never been tried before. The activity was investigated on cells infected with viral loads (MOI) like those found in the nose/upper airways in the initial phase of human infection [27]. Indeed, a review paper reported MOI values ranging from 0.001 to 2 for in vitro models of SARS-CoV-2 infection, using various cell lines [67]. After a series of preliminary experiments at higher MOIs (0.2 and 0.8), the ratios eventually applied in this study were 0.005 and 0.05.

It was decided not to deposit the solid powders as such directly on the cultured cells to avoid osmotic effects and uncontrolled CqP concentration in the well. Each powder was dissolved in culture medium at three test concentrations (25, 50 and 75 µM) to assess the effect of CqP concentration on the inhibition of viral replication. The cytotoxicity study on cells not infected with the virus, proved that CqP solutions in the 10–100 µM range did not cause cell death.

In the experiments with the virus, the infected cells were treated according to four protocols considering as variables the number of drug treatments post-infection (all protocols) and the addition of one treatment prior to the viral inoculum (protocols C and D).

SARS-CoV-2 inhibition was dependent on CqP concentration (protocols A-B)

The drug treatment was applied after cell infection one time or for 3 consecutive times at 2 h intervals. These protocols respectively mimic the single or multiple intranasal applications in already infected individuals. Figure 11 shows for both protocols A-B the antiviral effect of the three powders at the highest MOI (0.05), expressed as % of viral replication inhibition.

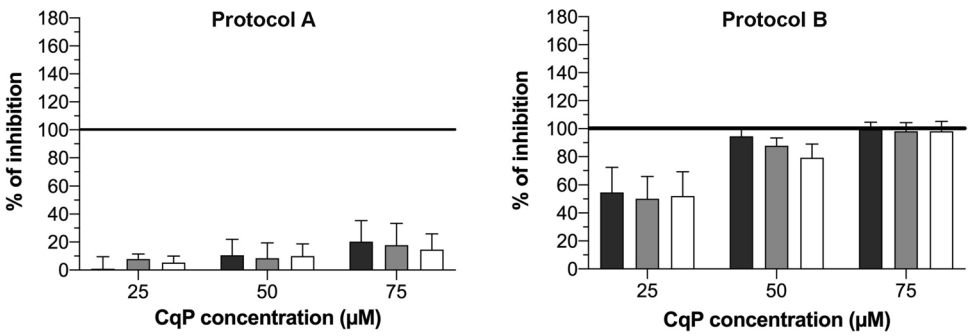

Fig. 11 Inhibition of SARS-CoV-2 replication (MOI 0.05) as a function of CqP concentration after 1 (left) or 3 (right) treatments post-infection: CqP monocomponent (black); CqP binary composite (grey); CqP ternary composite (white) (mean ± SEM; n ≥ 3). The straight line visually indicates 100% inhibition

For both protocols A-B, an increasing trend in the percent inhibition of viral replication was observed in dependence of CqP concentration, but the differences among the three concentration levels were not statistically significant for none of the compositions ($p > 0.05$ in all comparisons). In the present work, viral inhibition was assessed at CqP concentrations about 5–10 times as higher as the published IC_{50}. The in vitro activity of CqP against SARS-CoV-2 has been reported by different authors, with IC_{50} ranging between 1.13 and 5.47 μM at various MOIs [63, 68–70]. Some authors justified these data in terms of increased viral infectivity or different virus strain/variant [69].

By repeating the drug treatment post-infection (Protocol B), the % inhibition substantially improved and reached close to 100% inhibition with three treatments at 50 μM CqP. For sake of clarity, 100% inhibition corresponds to no difference in the amount of viral RNA between drug-treated cells and the untreated control at 48 h post-infection. For all powder compositions, the improvement due to repeated treatments with the CqP powders, was statistically significant ($p < 0.05$) for the 2 highest CqP concentrations. The translation of this microbiological result to the nasal therapy of a viral infection, recommends that repeated applications will be needed at suitable frequency, also to support the limited residence time in the upper airways.

The powder composition did not substantially affect the inhibitory activity of chloroquine diphosphate at the concentrations tested. In fact, neither zinc gluconate alone nor combined with lactoferrin resulted in a greater in vitro inhibition of SARS-CoV-2, compared to the CqP monocomponent powder. At some extent, these components seemed to slightly reduce the inhibitory effect of CqP, particularly the association zinc/lactoferrin in the ternary composite. However, none of such small differences was statistically significant ($p > 0.05$). As said, the combination of CqP with a zinc salt relied on the concept of CqP acting as Zn^{2+} ionophore [38, 64]. In the cytosol the metal element would inhibit RNA-dependent RNA polymerase and ultimately interfere with viral replication [71, 72]. As for lactoferrin, it was added to the nasal powder composition mainly to promote mucoadhesion [42, 43, 73]. According to the literature, lactoferrin could also have antiviral action per se [45, 74], which was not evidenced here. In summary, despite the enhanced accumulation of CqP in the rabbit mucosa ex vivo (Fig. 9), the hypothesized enhancement of the antiviral activity of chloroquine diphosphate by the additives zinc gluconate and lactoferrin did not occur in Vero E6 cells infected with SARS-CoV-2. It was verified that in the present study the actual concentration of both additives in the solutions used for cell treatment, were significantly lower as compared to active concentrations against SARS-CoV-2 reported in the literature [74, 75].

SARS-CoV-2 inhibition by CqP was enhanced when the cells were pre-treated before virus inoculum (protocols C-D)

Treatment protocols C and D were designed to assess whether pre-treating the cells with the drug before infection, affected the inhibitory effect. Figure 12 reports the % of viral replication inhibition at 0.05 MOI of the three nasal powders following these protocols.

As seen without pre-treatment, the effect of CqP concentration on the % of inhibition showed a similar increasing trend. In particular, when applying protocol D with the pre-treatment followed by 3 treatments post-infection, the increase in CqP concentration from 25 to 50 μM led to statistically significant higher inhibition ($p < 0.05$) for all three compositions. Moreover, CqP antiviral activity was not enhanced by the addition of zinc gluconate with or without lactoferrin to the powder composition.

Focusing on the actual benefit of the pre-treatment, in general the 2-h contact between cells and drug before virus inoculum increased the antiviral effect of the subsequent treatment/s performed after infection. In fact, the % inhibition values increased by 3–4 folds changing from protocol A to C or by 1.5 folds from protocol B to D. Notably, the enhancement provided by the pre-treatment with the drug was greater when only one treatment was performed post-infection and statistically significant ($p < 0.05$) in most cases.

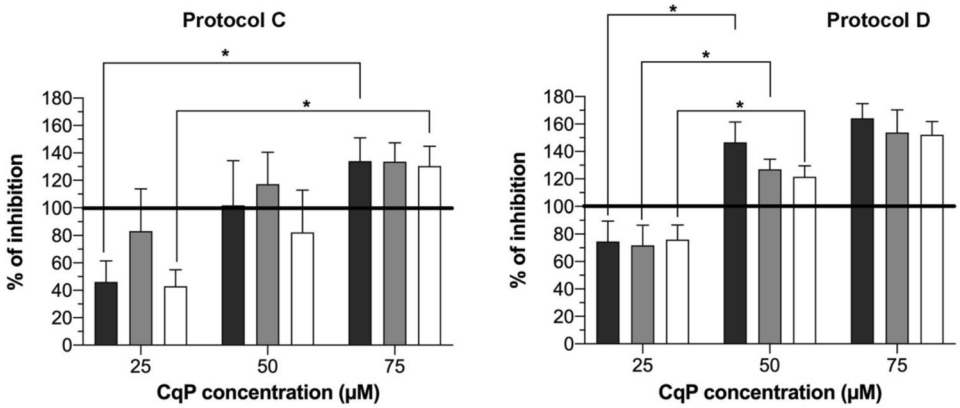

Fig. 12 Inhibition of SARS-CoV-2 replication (MOI 0.05) as a function of CqP concentration after drug treatment before virus inoculum (pre-treatment), followed by 1 (left) or 3 (right) treatments post-infection: CqP monocomponent (black); CqP binary composite (grey); CqP ternary composite (white) (mean ± SEM; $n \geq 3$). The straight line visually indicates 100% inhibition. The asterisk indicates statistical significance ($p < 0.05$)

In the comparison of the % inhibition values of protocols B *vs.* D, the enhancement was statistically significant for all powder compositions at 50 and 75 μM CqP ($p < 0.05$). As a final remark, the drug pre-treatment made one treatment post-infection (Fig. 12-left) as effective as the three treatments post-infection without pre-treatment (Fig. 11-right).

The reader unfamiliar with Ct-based quantification of % of inhibition, may misinterpret that at 50 and 75 μM CqP, % inhibition was often > 100% with the pre-treatment. Indeed, these values result from an increase of the cycle threshold (Ct) value for the treated cells at 48 h compared to the Ct value of virus control. Consequently, they reflect relative Ct shifts rather than absolute inhibition. They indicate that viral RNA lysis occurred as a consequence of the drug treatment. The lysis might have been caused by a metabolic activity of the cell that eventually destroyed a virus weakened by the repeated drug action. Nevertheless, percent inhibition values equal to or higher than 100% have to be considered equivalent in terms of antiviral activity.

Two papers have reviewed the possible mechanisms by which antimalarial chloroquine and hydroxychloroquine may act as antiviral drugs, not only against SARS-CoV-2. On one hand both could interfere with viral attachment and entry into the host cell. In addition, they may hinder the maturation and spread of the new viral particles [17, 76]. Our experiments showed an effect of CqP on SARS-CoV-2 replication that depended on when the drug was applied with respect to the infection time. When applied only after the infection (protocols A-B), CqP likely found the virus already in the cell under replication and the inhibitory effect was lower. In contrast, the enhancement observed with the pre-treatment, is substantiated by the presence of CqP inside and outside the cell when the virus was inoculated. Thereby, additional mechanisms might justify the observed stronger inhibition [17]. In this regard, we evidenced a mild inhibitory effect (10–30% inhibition *vs.* untreated virus control) by all powders in a single experiment in which the cells were only pre-treated and no drug treatment followed after infection (data not shown). The inhibition by the pre-treatment alone was in the same order of magnitude of the effect of one treatment post-infection (protocol A), corroborating the idea that CqP acts based on a combination of pre- and post-entry antiviral mechanisms.

At the lowest MOI (0.005), the percent inhibition measured applying the same protocols and CqP concentrations was substantially the same observed at 0.05 MOI. Increasing the CqP concentration made the inhibition stronger, although statistically significant only for the ternary composite from 25 to 75 μM ($p < 0.05$). Also, pre-treating the cells with the drug significantly enhanced CqP antiviral activity ($p < 0.05$) for protocol C at the two highest drug concentrations. The four bar graphs for these experiments are reported as Supplementary Material (Fig. S3).

As a final remark about the three nasal powder compositions, their substantially similar effect could be due to the fact of testing the potential contribution by Zn^{2+} and lactoferrin at CqP concentrations where the high drug activity may have hidden any effect by the combined agents.

Conclusions and perspectives

In airborne diseases by respiratory viruses, nasal antiviral powders could provide a therapeutical tool to close the gap existing between symptom appearance and treatment onset of the early infection in the upper airways. The loco-regional deposition of small doses of chloroquine diphosphate aerodynamic particles provided fast drug dissolution and absorption by the nasal mucosa, determining much higher intraepithelial drug concentrations than the published in vitro antiviral IC_{50}. Moreover, the observed in vitro anti SARS-CoV-2 activity of CqP composite powders and the benefit of in vitro cell pre-treatment with the drug before infection, broadens the use of this nasal powder product envisaging a preventive treatment for subjects at risk of infection. The contribution of the additives in binary and ternary composites was significant for the ex vivo accumulation of CqP in the rabbit nasal mucosa, but not for the inhibition of viral replication in vitro, due to their low concentration and predominant CqP activity.

The in vivo study with the mannitol powder and Turbospin® device in humans, showed that a dose of respirable powder can be quantitatively extracted in aerosol form and deposited onto the upper airways beyond the throat, as evidenced by the sweet taste of mannitol perceived by the volunteers. After assuring nasal powder reproducibility and stability, product development can enter the preclinical phase in a relevant animal model to assess deposition in vivo, local tolerability, systemic exposure and safety.

Prospectively, sniffing a nasal antiviral powder could timely treat the patient and prevent disease worsening to pneumonia. It is also not unrealistic that the loco-regional antiviral action might reduce the contagiousness of infected subjects. Looking ahead, the studied nasal powder prototypes meet the patient need to find in retail pharmacy an active and safe medicine for use at home, promptly prescribed by the general practitioner at first infection symptoms. To use such a product, the patients will only need to be trained by the pharmacist to perform the correct nasal inhalation maneuver. The antiviral medicine can thus target three categories of subjects:

1. early infected symptomatic subjects, to directly and promptly attack the virus replication in the upper airways;
2. asymptomatic infected subjects, to control their potential infectiveness;

3. subjects exposed to virus contamination for work reason (e.g. doctors, nurses, caregivers), to protect them from infection.

Even though the COVID-19 pandemic ended, the meaningfulness of the presented drug release strategy remains valid because other viral airborne diseases exist and other antiviral drugs can be candidate to the nasal inhalation route. The ultimate goal is to target the deposition all over the upper airways of the selected antiviral drug formulated as an aerodynamic powder, favorably performing in the nasal breath-powered administration. Finally, this medicine administration copies the same virus entry and route.

Supplementary Information The online version contains supplementary material available at https://doi.org/10.1007/s13346-025-01916-7.

Acknowledgements We owe heartfelt gratitude to the >200 individuals, associations and companies whose liberal donations and belief in our research made this study possible. Their support through the 2021 crowdfunding campaign of the University of Ferrara in response to the COVID-19 pandemic, has been instrumental in advancing the work. Their generosity and trust highlight the essential link between the scientific community and society at large. Among them, the F.A.I (Federazione Autotrasportatori Italiani) donated in memory of Duilio Balducchi (F.A.I. Honorary President) and Roberto Grechi (President of Ferrara F.A.I. section), both victims of COVID-19. Finally, together with the "Gruppo Alpini di Cento", we dedicate this paper to the memory of Capitano Massimo Ranzani of the 5th Alpine Troopers Regiment, who lost his life in 2011 during a military mission in Afghanistan. His sacrifice reminds us all of the importance of service, dedication, and the pursuit of a greater good for mankind.

Author contribution All authors contributed to the study conception and design. Material preparation, data collection and analysis were performed by Sabrina Banella and Eride Quarta who equally contributed to the work. Further investigation was carried out by Martina Brandolini, Laura Grumiro, Giovanna Trevisi and Georgeta Caraua. Francesca Buttini, Fabio Sonvico and Alessandra Rossi were involved in Data curation and specific Methodology issues. Vittorio Sambri, Ruggero Bettini and Gaia Colombo provided resources and funding. The first draft of the manuscript was written by Sabrina Banella, Paolo Colombo and Gaia Colombo. All authors commented on previous versions of the manuscript. All authors read and approved the final manuscript.

Funding This research did not receive any specific grant from funding agencies in the public, commercial, or not-for-profit sectors. Nevertheless, it was supported by liberal donations raised during the 2021 crowdfunding campaign of the University of Ferrara.

Data availability The datasets generated and analyzed during the current study are available from the corresponding author on reasonable request.

Declarations

Ethics approval This study was performed in line with the principles of the Declaration of Helsinki. Approval was granted by the Research Ethics Board of the University of Parma (June 11th, 2024, protocol number 0145714).

Informed consent All procedures followed were in accordance with the ethical standards of the responsible committee on human experimentation (institutional and national) and with the Helsinki Declaration of 1975, as revised in 2000. Informed consent was obtained from all healthy volunteers for being included in the study.

Competing interest Emeritus Professor Paolo Colombo is the administrator of the innovative SME PlumeStars s.r.l., the Applicant of an Italian patent on "Novel Antiviral Compositions and Their Use in Therapy and in the Treatment of Viral Infections" (No. 102021000002003, filed on 01/02/2021). Paolo Colombo, Eride Quarta, Gaia Colombo and Sabrina Banella are the inventors of that patent. Ruggero Bettini and Francesca Buttini, both professors of Pharmaceutical Technology at the Food and Drug Department of the University of Parma, are co-founders of PlumeStars start-up. The other authors have no relevant financial or non-financial interests to disclose.

References

1. Siddiqi HK, Mehra MR. COVID-19 illness in native and immunosuppressed states: a clinical-therapeutic staging proposal. J Heart Lung Transplant. 2020;39(5):405–7. https://doi.org/10.1016/j.healun.2020.03.012.
2. Gaziano L, Giambartolomei C, Pereira AC, Gaulton A, Posner DC, Swanson SA, Ho YL, Iyengar SK, Kosik NM, Vujkovic M, Gagnon DR, Bento AP, Barrio-Hernandez I, Rönnblom L, Hagberg N, Lundtoft C, Langenberg C, Pietzner M, Valentine D, Gustincich S, Tartaglia GG, Allara E, Surendran P, Burgess S, Zhao JH, Peters JE, Prins BP, Angelantonio ED, Devineni P, Shi Y, Lynch KE, DuVall SL, Garcon H, Thomann LO, Zhou JJ, Gorman BR, Huffman JE, O'Donnell CJ, Tsao PS, Beckham JC, Pyarajan S, Muralidhar S, Huang GD, Ramoni R, Beltrao P, Danesh J, Hung AM, Chang KM, Sun YV, Joseph J, Leach AR, Edwards TL, Cho K, Gaziano JM, Butterworth AS, Casas JP, VA Million Veteran Program COVID-19 Science Initiative. Actionable druggable genome-wide Mendelian randomization identifies repurposing opportunities for COVID-19. Nat Med. 2021;27(4):668–676. https://doi.org/10.1038/s41591-021-01310-z
3. Ng YL, Salim CK, Chu JJH. Drug repurposing for COVID-19: approaches, challenges and promising candidates. Pharmacol Ther. 2021;228:107930. https://doi.org/10.1016/j.pharmthera.2021.107930.
4. Weis N, Bollerup S, Sund JD, Glamann JB, Vinten C, Jensen LR, Sejling C, Kledal TN, Rosenkilde MM. Amantadine for COVID-19 treatment (ACT) study: a randomized, double-blinded, placebo-controlled clinical trial. Clin Microbiol Infect. 2023;29(10):1313–9. https://doi.org/10.1016/j.cmi.2023.06.023.
5. Cheema HA, Jafar U, Shahid A, Masood W, Usman M, Hermis AH, Naseem MA, Sahra S, Sah R, Lee KY. Colchicine for the treatment of patients with COVID-19: an updated systematic review and meta-analysis of randomised controlled trials. BMJ Open. 2024;14(4): e074373. https://doi.org/10.1136/bmjopen-2023-074373.
6. WHO COVID-19 Solidarity Therapeutics Trial. https://www.who.int/emergencies/diseases/novel-coronavirus-2019/global-research-on-novel-coronavirus-2019-ncov/solidarity-clinical-trial-for-covid-19-treatments, 2021. Accessed 11 March 2025.
7. Recovery trial. https://www.recoverytrial.net/, 2023. Accessed 11 March 2025.
8. Godwin PO, Polsonetti B, Caron MF, Oppelt TF. Remdesivir for the treatment of COVID-19: a narrative review. Infect Dis Ther. 2024;13(1):1–19. https://doi.org/10.1007/s40121-023-00900-3.

9. European Centre for Disease Prevention and Control (ECDC). Antiviral treatment of influenza. https://www.ecdc.europa.eu/en/seasonal-influenza/prevention-and-control/antivirals, 2023. Accessed 11 March 2025.
10. Seow HC, Liao Q, Lau ATY, Leung SWS, Yuan S, Lam JKW. Dual targeting powder formulation of antiviral agent for customizable nasal and lung deposition profile through single intranasal administration. Int J Pharm. 2022;619: 121704. https://doi.org/10.1016/j.ijpharm.2022.121704.
11. Sonvico F, Colombo G, Quarta E, Guareschi F, Banella S, Buttini F, Scherließ R. Nasal delivery as a strategy for the prevention and treatment of COVID-19. Expert Opin Drug Deliv. 2023;20(8):1115–30. https://doi.org/10.1080/17425247.2023.2263363.
12. Muñoz-Prieto A, Contreras-Aguilar MD, Cerón JJ, Ayala I, Martin-Cuervo M, Gonzalez-Sanchez JC, Jacobsen S, Kuleš J, Beletić A, Rubić I, Mrljak V, Tecles F, Hansen S. Changes in proteins in saliva and serum in Equine gastric ulcer syndrome using a proteomic approach. Animals. 2022;12(9):1169. https://doi.org/10.3390/ani12091169.
13. Shilts MH, Rosas-Salazar C, Strickland BA, Kimura KS, Asad M, Sehanobish E, Freeman MH, Wessinger BC, Gupta V, Brown HM, Boone HH, Patel V, Barbi M, Bottalico D, O'Neill M, Akbar N, Rajagopala SV, Mallal S, Phillips E, Turner JH, Jerschow E, Das SR. Severe COVID-19 Is Associated With an Altered Upper Respiratory Tract Microbiome. Front Cell Infect Microbiol. 2022;11:781968. https://doi.org/10.3389/fcimb.2021.781968.
14. Wilding RJ, Thynne M, Subhan MMF. Optimization of sniff nasal inspiratory pressure (SNIP) measurement methodology in healthy subjects. BMC Pulm Med. 2023;23:66. https://doi.org/10.1186/s12890-023-02348-0.
15. Savarino A, Boelaert JR, Cassone A, Majori G, Cauda R. Effects of chloroquine on viral infections: an old drug against today's diseases? Lancet Infect Dis. 2003;3(11):722–7. https://doi.org/10.1016/s1473-3099(03)00806-5.
16 Meo SA, Klonoff DC, Akram J. Efficacy of chloroquine and hydroxychloroquine in the treatment of COVID-19. Eur Rev Med Pharmacol Sci. 2020;24(8):4539–47. https://doi.org/10.26355/eurrev_202004_21038.
17. Carafoli E. Chloroquine and hydroxychloroquine in the prophylaxis and therapy of COVID-19 infection. Biochem Biophys Res Commun. 2021;538:156–62. https://doi.org/10.1016/j.bbrc.2020.09.128.
18. Martinelli F, Balducci AG, Rossi A, Sonvico F, Colombo P, Buttini F. Pierce and inhale" design in capsule based dry powder inhalers: Effect of capsule piercing and motion on aerodynamic performance of drugs. Int J Pharm. 2015;487(1–2):197–204. https://doi.org/10.1016/j.ijpharm.2015.04.003.
19. Cui C, Zhang M, Yao X, Tu S, Hou Z, Jie En VS, Xiang X, Lin J, Cai T, Shen N, Song C, Qiao J, Zhang S, Li H, Liu D. Dose selection of chloroquine phosphate for treatment of COVID-19 based on a physiologically based pharmacokinetic model. Acta Pharm Sin B. 2020;10(7):1216–27. https://doi.org/10.1016/j.apsb.2020.04.007.
20. Buttini F, Cuoghi E, Miozzi M, Rossi A, Sonvico F, Colombo P. Insulin spray-dried powder and smoothed lactose: a new formulation strategy for nasal and pulmonary delivery. Respir Drug Deliv. 2012;3:835–40.
21. Müller D, Fimbinger E, Brand C. Algorithm for the determination of the angle of repose in bulk material analysis. Powder Technol. 2021;383:598–605. https://doi.org/10.1016/j.powtec.2021.01.010.
22. Quarta E, Chierici V, Flammini L, Tognolini M, Barocelli E, Cantoni AM, Dujovny G, Ecenarro Probst S, Sonvico F, Colombo G, Rossi A, Bettini R, Colombo P, Buttini F. Excipient-free pulmonary insulin dry powder: pharmacokinetic and pharmacodynamics profiles in rats. J Control Release. 2020;323:412–20. https://doi.org/10.1016/j.jconrel.2020.04.015.
23. Buttini F, Balducci AG, Colombo G, Sonvico F, Montanari S, Pisi G, Rossi A, Colombo P, Bettini R. Dose administration maneuvers and patient care in tobramycin dry powder inhalation therapy. Int J Pharm. 2018;548(1):182–91. https://doi.org/10.1016/j.ijpharm.2018.06.006.
24. Balducci AG, Ferraro L, Bortolotti F, Nastruzzi C, Colombo P, Sonvico F, Russo P, Colombo G. Antidiuretic effect of desmopressin chimera agglomerates by nasal administration in rats. Int J Pharm. 2013;440(2):154–60. https://doi.org/10.1016/j.ijpharm.2012.09.049.
25. Tiozzo Fasiolo L, Manniello MD, Bortolotti F, Buttini F, Rossi A, Sonvico F, Colombo P, Valsami G, Colombo G, Russo P. Anti-inflammatory flurbiprofen nasal powders for nose-to-brain delivery in Alzheimer's disease. J Drug Target. 2019;27(9):984–94. https://doi.org/10.1080/1061186X.2019.1574300.
26. Choi KY, Cho SW, Choi JJ, Zhang YL, Kim DW, Han DH, Kim HJ, Kim DY, Rhee CS, Won TB. Healing of the nasal septal mucosa in an experimental rabbit model of mucosal injury. World Journal of Otorhinolaryngology. 2017;3(1):17–23. https://doi.org/10.1016/j.wjorl.2017.02.004.
27. Johnson TJ, Nishida RT, Sonpar AP, Lin YJ, Watson KA, Smith SW, Conly JM, Evans DH, Olfert JS. Viral load of SARS-CoV-2 in droplets and bioaerosols directly captured during breathing, speaking and coughing. Sci Rep. 2022;12(1):3484. https://doi.org/10.1038/s41598-022-07301-5.
28. Pujadas E, Chaudhry F, McBride R, Richter F, Zhao S, Wajnberg A, Nadkarni G, Glicksberg BS, Houldsworth J, Cordon-Cardo C. SARS-CoV-2 viral load predicts COVID-19 mortality. Lancet Respir Med. 2020;8(9):e70. https://doi.org/10.1016/S2213-2600(20)30354-4.
29. Marc A, Kerioui M, Blanquart F, Bertrand J, Mitjà O, Corbacho-Monné M, Marks M, Guedj J. Quantifying the relationship between SARS-CoV-2 viral load and infectiousness. Elife. 2021;10: e69302. https://doi.org/10.7554/eLife.69302.
30. Kiryanov SA, Levina TA, Konopleva MV, Suslov AP. Identification of hotspot mutations in the N gene of SARS-CoV-2 in Russian clinical samples that may affect the detection by reverse transcription-PCR. Diagnostics. 2022;12(1):147. https://doi.org/10.3390/diagnostics12010147.
31. Brandolini M, Taddei F, Marino MM, Grumiro L, Scalcione A, Turba ME, Gentilini F, Fantini M, Zannoli S, Dirani G, Sambri V. Correlating qRT-PCR, dPCR and viral titration for the identification and quantification of SARS-CoV-2: a new approach for infection management. Viruses. 2021;13(6):1022. https://doi.org/10.3390/v13061022.
32. Banella S, Saraswat A, Patel A, Serajuddin ATM, Colombo P, Patel K, Colombo G. In vitro assessment of Cisplatin/Hyaluronan complex for loco-regional chemotherapy. Int J Mol Sci. 2023;24(21):15725. https://doi.org/10.3390/ijms242115725.
33. Claes E, Wener R, Neyrinck AP, Coppens A, Van Schil PE, Janssens A, Lapperre TS, Snoeckx A, Wen W, Voet H, Verleden SE, Hendriks JMH. Innovative invasive loco-regional techniques for the treatment of lung cancer. Cancers (Basel). 2023;15(8):2244. https://doi.org/10.3390/cancers15082244.
34. Colson P, Rolain JM, Raoult D. Chloroquine for the 2019 novel coronavirus SARS-CoV-2. Int J Antimicrob Agents. 2020;55(3):105923. https://doi.org/10.1016/j.ijantimicag.2020.105923.
35. Browning DJ. Pharmacology of Chloroquine and Hydroxychloroquine. In: D.J. Browning DJ, editor. Hydroxychloroquine and Chloroquine Retinopathy. New York: Springer; 2014. pp. 35–63. https://doi.org/10.1007/978-1-4939-0597-3_2
36. Sheahan TP, Sims AC, Zhou S, Graham RL, Pruijssers AJ, Agostini ML, Leist SR, Schäfer A, Dinnon 3rd KH, Stevens LJ,

Chappell JD, Lu X, Hughes TM, George AS, Hill CS, Montgomery SA, Brown AJ, Bluemling GR, Natchus MG, Saindane M, Kolykhalov AA, Painter G, Harcourt J, Tamin A, Thornburg NJ, Swanstrom R, Denison MR, Baric RS. An orally bioavailable broad-spectrum antiviral inhibits SARS-CoV-2 in human airway epithelial cell cultures and multiple coronaviruses in mice. Sci. Transl. Med. 2020;12:eabb5883. https://doi.org/10.1126/scitranslmed.abb5883

37. Saravolatz LD, Depcinski S, Sharma M. Molnupiravir and Nirmatrelvir-Ritonavir: Oral Coronavirus Disease 2019. Antiviral Drugs, Clin Infect Dis. 2023;76(1):165–71. https://doi.org/10.1093/cid/ciac180.
38. Xue J, Moyer A, Peng B, Wu J, Hannafon BN, Ding WQ. Chloroquine is a zinc ionophore. PLoS ONE. 2014;9(10): e109180. https://doi.org/10.1371/journal.pone.0109180.
39. Porowska A, Dosta M, Fries L, Gianfrancesco A, Heinrich S, Palzer S. Predicting the surface composition of a spray-dried particle by modelling component reorganization in a drying droplet. Chem Eng Res Des. 2016;110:131–40. https://doi.org/10.1016/j.cherd.2016.03.007.
40. England RJ, Homer JJ, Knight LC, Ell SR. Nasal pH measurement: a reliable and repeatable parameter. Clin Otolaryngol Allied Sci. 1999;24(1):67–8. https://doi.org/10.1046/j.1365-2273.1999.00223.x.
41. Washington N, Steele RJ, Jackson SJ, Bush D, Mason J, Gill DA, Pitt K, Rawlins DA. Determination of baseline human nasal pH and the effect of intranasally administered buffers. Int J Pharm. 2000;198(2):139–46. https://doi.org/10.1016/s0378-5173(99)00442-1.
42 Leal J, Smyth HDC, Ghosh D. Physicochemical properties of mucus and their impact on transmucosal drug delivery. Int J Pharm. 2017;532(1):555–72. https://doi.org/10.1016/j.ijpharm.2017.09.018.
43. Szilágyi BÁ, Mammadova A, Gyarmati B, Szilágyi A. Mucoadhesive interactions between synthetic polyaspartamides and porcine gastric mucin on the colloid size scale. Colloids Surf B Biointerfaces. 2020;194: 111219. https://doi.org/10.1016/j.colsurfb.2020.111219.
44. van der Strate BW, Beljaars L, Molema G, Harmsen MC, Meijer DK. Antiviral activities of lactoferrin. Antivir Res. 2001;52(3):225–39. https://doi.org/10.1016/s0166-3542(01)00195-4.
45. Campione E, Lanna C, Cosio T, Rosa L, Conte MP, Iacovelli F, Romeo A, Falconi M, Del Vecchio C, Franchin E, Lia MS, Minieri M, Chiaramonte C, Ciotti M, Nuccetelli M, Terrinoni A, Iannuzzi I, Coppeda L, Magrini A, Bernardini S, Sabatini S, Rosapepe F, Bartoletti PL, Moricca N, Di Lorenzo A, Andreoni M, Sarmati L, Miani A, Piscitelli P, Valenti P, Bianchi L. Lactoferrin against SARS-CoV-2. In vitro and in silico evidences. Front Pharmacol. 2021;12:666600. https://doi.org/10.3389/fphar.2021.666600.
46. Ong R, Cornish J, Wen J. Nanoparticular and other carriers to deliver lactoferrin for antimicrobial, antibiofilm and bone-regenerating effects: a review. Biometals. 2023;36(3):709–27. https://doi.org/10.1007/s10534-022-00455-9.
47. Le Guellec S, Ehrmann S, Vecellio L. In vitro - in vivo correlation of intranasal drug deposition. Adv Drug Deliv Rev. 2021;170:340–52. https://doi.org/10.1016/j.addr.2020.09.002.
48. Pozzoli M, Rogueda P, Zhu B, Smith T, Young PM, Traini D, Sonvico F. Dry powder nasal drug delivery: challenges, opportunities and a study of the commercial Teijin Puvlizer Rhinocort device and formulation. Drug Dev Ind Pharm. 2016;42(10):1660–8. https://doi.org/10.3109/03639045.2016.1160110.
49. Morrison CB, Edwards CE, Shaffer KM, Araba KC, Wykoff JA, Williams DR, Asakura T, Dang H, Morton LC, Gilmore RC, O'Neal WK, Boucher RC, Baric RS, Ehre C. SARS-CoV-2 infection of airway cells causes intense viral and cell shedding, two spreading mechanisms affected by IL-13. Proc Natl Acad Sci U S A. 2022;119(16): e2119680119. https://doi.org/10.1073/pnas.2119680119.
50. Bridges JP, Vladar EK, Huang H, Mason RJ. Respiratory epithelial cell responses to SARS-CoV-2 in COVID-19. Thorax. 2022;77(2):203–9. https://doi.org/10.1136/thoraxjnl-2021-217561.
51. European Pharmacopoeia 11th ed., 2.9.36. Powder Flow (07/2024), Suppl. 11.5: 5834–5836.
52. Beakawi Al-Hashemi HM, Baghabra Al-Amoudi OS. A review on the angle of repose of granular materials. Powder Technol. 2018;330:397–417. https://doi.org/10.1016/j.powtec.2018.02.003.
53. Vehring R, Foss WR, Lechuga-Ballesteros D. Particle formation in spray drying. J Aerosol Sci. 2007;38:728–46. https://doi.org/10.1016/j.jaerosci.2007.04.005.
54. Capstick TGD, Gudimetla S, Harris DS, Malone R, Usmani OS. Demystifying dry powder inhaler resistance with relevance to optimal patient care. Clin Drug Investig. 2024;44(2):109–14. https://doi.org/10.1007/s40261-023-01330-2.
55. Ung KT, Chan HK. Effects of ramp-up of inspired airflow on in vitro aerosol dose delivery performance for certain dry powder inhalers. Eur J Pharm Sci. 2016;10(84):46–54. https://doi.org/10.1016/j.ejps.2016.01.005.
56. Finlay WH, Darquenne C. Particle size distributions. J Aerosol Med Pulm Drug Deliv. 2020;33(4):178–80. https://doi.org/10.1089/jamp.2020.29028.whf.
57. Saha T, Quiñones-Mateu ME, Das SC. Inhaled therapy for COVID-19: considerations of drugs, formulations and devices. Int J Pharm. 2022;624:122042. https://doi.org/10.1016/j.ijpharm.2022.122042.
58. Sahakijpijarn S, Moon C, Warnken ZN, Maier EY, DeVore JE, Christensen DJ, Koleng JJ, Williams RO 3rd. In vivo pharmacokinetic study of remdesivir dry powder for inhalation in hamsters. Int J Pharm X. 2021;3: 100073. https://doi.org/10.1016/j.ijpx.2021.100073.
59. de Reus YA, Hagedoorn P, Sturkenboom MGG, Grasmeijer F, Bolhuis MS, Sibum I, Kerstjens HAM, Frijlink HW, Akkerman OW. Tolerability and pharmacokinetic evaluation of inhaled dry powder hydroxychloroquine in healthy volunteers. PLoS ONE. 2022;17(8): e0272034. https://doi.org/10.1371/journal.pone.0272034.
60. Daneshfar A, Vafafard S. Solubility of chloroquine diphosphate and 4,7-dichloroquinoline in water, ethanol, tetrahydrofuran, acetonitrile, and acetone from (298.2 to 333.2) K. J Chem Eng Data. 2009;54(8):2170–3. https://doi.org/10.1021/je8007099.
61. Frenning G, van der Zwaan I, Franek F, Fransson R, Tehler U. Model for the analysis of membrane-type dissolution tests for inhaled drugs. Mol Pharm. 2020;17(7):2426–34. https://doi.org/10.1021/acs.molpharmaceut.0c00163.
62. Tiozzo Fasiolo L, Manniello MD, Tratta E, Buttini F, Rossi A, Sonvico F, Bortolotti F, Russo P, Colombo G. Opportunity and challenges of nasal powders: drug formulation and delivery. Eur J Pharm Sci. 2018;113:2–17. https://doi.org/10.1016/j.ejps.2017.09.027.
63. Yao X, Ye F, Zhang M, Cui C, Huang B, Niu P, Liu X, Zhao L, Dong E, Song C, Zhan S, Lu R, Li H, Tan W, Liu D. In vitro antiviral activity and projection of optimized dosing design of hydroxychloroquine for the treatment of severe acute respiratory syndrome coronavirus 2 (SARS-CoV-2). Clin Infect Dis. 2020;71(15):732–9. https://doi.org/10.1093/cid/ciaa237.
64. Hu Y, Li YV. The change of intracellular zinc distribution after strong acid challenge. Int J Physiol Pathophysiol Pharmacol. 2021;13(3):94–101.
65. González-Chávez SA, Arévalo-Gallegos S, Rascón-Cruz Q. Lactoferrin: structure, function and applications. Int J Antimicrob

Agents. 2009;33(4):301.e1-8. https://doi.org/10.1016/j.ijantimicag.2008.07.020.
66. Essaidi-Laziosi M, Perez Rodriguez FJ, Hulo N, Jacquerioz F, Kaiser L, Eckerle I. Estimating clinical SARS-CoV-2 infectiousness in Vero E6 and primary airway epithelial cells. Lancet Microbe. 2021;2(11): e571. https://doi.org/10.1016/S2666-5247(21)00216-0.
67. Rosa RB, Dantas WM, do Nascimento JFC, da Silva MV, de Oliveira RN, Pena LJ. In Vitro and In Vivo Models for Studying SARS-CoV-2, the Etiological Agent Responsible for COVID-19 Pandemic. Viruses 2021;13(3):379. https://doi.org/10.3390/v13030379
68. Wang M, Cao R, Zhang L, Yang X, Liu J, Xu M, Shi Z, Hu Z, Zhong W, Xiao G. Remdesivir and chloroquine effectively inhibit the recently emerged novel coronavirus (2019-nCoV) *in vitro*. Cell Res. 2020;30(3):269–71. https://doi.org/10.1038/s41422-020-0282-0.
69. Liu J, Cao R, Xu M, Wang X, Zhang H, Hu H, Li Y, Hu Z, Zhong W, Wang M. Hydroxychloroquine, a less toxic derivative of chloroquine, is effective in inhibiting SARS-CoV-2 infection in vitro. Cell Discov. 2020;6:16. https://doi.org/10.1038/s41421-020-0156-0.
70. Gendrot M, Andreani J, Boxberger M, Jardot P, Fonta I, Le Bideau M, Duflot I, Mosnier J, Rolland C, Bogreau H, Hutter S, La Scola B, Pradines B. Antimalarial drugs inhibit the replication of SARS-CoV-2: an in vitro evaluation. Travel Med Infect Dis. 2020;37:101873. https://doi.org/10.1016/j.tmaid.2020.101873.
71. Shittu MO, Afolami OI. Improving the efficacy of Chloroquine and Hydroxychloroquine against SARS-CoV-2 may require Zinc additives - A better synergy for future COVID-19 clinical trials. Le Infezioni in Medicina; 2020;28(2):192–197. https://infezmed.it/media/journal/Vol_28_2_2020_9.pdf Accessed 17 March 2025.
72. Derwand R, Scholz M. Does zinc supplementation enhance the clinical efficacy of chloroquine/hydroxychloroquine to win today's battle against COVID-19? Med Hypotheses. 2020;142: 109815. https://doi.org/10.1016/j.mehy.2020.109815.
73. Jiang L, Gao L, Wang X, Tang L, Ma J. The application of mucoadhesive polymers in nasal drug delivery. Drug Dev Ind Pharm. 2010;36(3):323–36. https://doi.org/10.1080/03639040903170750.
74. Hu Y, Meng X, Zhang F, Xiang Y, Wang J. The in vitro antiviral activity of lactoferrin against common human coronaviruses and SARS-CoV-2 is mediated by targeting the heparan sulfate co-receptor. Emerg Microbes Infect. 2021;10(1):317–30. https://doi.org/10.1080/22221751.
75. Tao X, Zhang L, Du L, Lu K, Zhao Z, Xie Y, Li X, Huang S, Wang PH, Pan JA, Xia W, Dai J, Mao ZW. Inhibition of SARS-CoV-2 replication by zinc gluconate in combination with hinokitiol. J Inorg Biochem. 2022;231: 111777. https://doi.org/10.1016/j.jinorgbio.2022.111777.
76. Quiros Roldan E, Biasiotto G, Magro P, Zanella I. The possible mechanisms of action of 4-aminoquinolines (chloroquine/hydroxychloroquine) against Sars-Cov-2 infection (COVID-19): a role for iron homeostasis? Pharmacol Res. 2020;158:104904. https://doi.org/10.1016/j.phrs.2020.104904.